SYNERGISTIC STUDY ON ELECTROCHEMICALLY DEPOSITED THIN FILM WITH A SPECTRUM FROM MICRO TO NANO RANGE STRUCTURES

A thesis submitted in partial fulfillment of the requirement for the award of degree of

Masters of Technology
In
Metallurgical and Materials Engineering

Submitted by

Anil Kumar Singh Bankoti

Roll No. 207MM108

Department of Metallurgical and Materials Engineering

National Institute of Technology,

Rourkela-769008,

2009

SYNERGISTIC STUDY ON ELECTROCHEMICALLY DEPOSITED THIN FILM WITH A SPECTRUM FROM MICRO TO NANO RANGE STRUCTURES

A thesis submitted in partial fulfillment of the requirement for the award of the degree of

Masters of Technology
In
Metallurgical and Materials Engineering

Submitted by

Anil Kumar Singh Bankoti

Roll No. 207MM108

Under the Supervision of

Prof. B.C. Ray **Mrs. Archana Mallik**

Department of Metallurgical and Materials Engineering

National Institute of Technology, Rourkela

National Institute of Technology

Rourkela

Certificate

This is to certify that the thesis entitled **"Synergistic study on electrochemically deposited thin film with a spectrum from micro- to nano range structures"** submitted by Mr. Anil Kumar Singh Bankoti in partial fulfillment of the requirements for the award of Masters of Technology in Metallurgical and Materials Engineering with specialization in "Metallurgical and Materials Engineering" at National Institute of Technology, Rourkela (Deemed University) is an authentic work carried out by him under our supervision and guidance.

To the best of our knowledge, the matter embodied in the thesis has not been submitted to any other university/Institute for the award any Degree or Diploma.

Supervisor
Prof. B.C.Ray
Metallurgical and Materials Engg.
National Institute of Technology,
Rourkela-769008

Co-Supervisor
Mrs. Archana Mallik
Management Trainee (Technical)
R & C Lab. SAIL
Rourkela-769008

Acknowledgement

I take this opportunity to express my deep regards and sincere gratitude for this valuable, expert guidance rendered to me by guide Dr. B. C. Ray, Professor, Department of Metallurgical and Materials Engineering, National Institute of Technology, Rourkela and Mrs. Archana Mallik, Management Trainee (Technical), R & C Lab, SAIL, Rourkela. I consider me fortunate to have had opportunity to work under their guidance and enrich myself from their vast knowledge and analysis power. They will always be constant source of inspiration for me.

My sincere thanks to Dr. B. B. Verma, Professor and Head Metallurgical and Materials engineering Department for his talented advice and providing necessary facility for my work.

I would also take this opportunity to express my gratitude and sincere thanks to my honorable teachers for their invaluable advice, constant help, encouragement, inspiration and blessing.

I am thankful to Dr. S. K. Pradhan, Scientist, IMMT Bhubaneswar, for his help during the sample characterization.

I am also thankful to laboratory members of Department of Metallurgical and Materials Engineering, NIT Rourkela, especially, R. Pattanaik, S. Pradhan, U. K. Sahu for constant practical assistance and help whenever required.

Special thanks to my friends and other members of the department for being so supportive and helpful in every possible way.

Anil Kumar Singh Bankoti

CONTENTS

LIST OF FIGURES

LIST OF TABLES

ABSTRACT

Thin films are deposited onto bulk materials (substrates) to achieve properties unattainable or not easily attainable in the substrates alone. The film thickness usually varies from few nanometers to a maximum value of 1 μm. Cavitation, irradiation of liquid with high intensity ultrasound, as a means of altering the crystallization process is achieved by the repeated creation and collapse of microscopic bubbles inside the solution. It is at the solid-liquid interface that electrochemical techniques may be employed to detect the possible influence of sonication on electrochemical nucleation and growth of clusters. In this work we prepare the copper thin film by sonoelectrosynthesis method at different temperature, acid and concentration of electrolyte. Films are characterized by XRD, SEM, AFM, and study of the mechanical properties is done by nanaoidentation. Scahifker and Hills model was used for study of nucleation and growth phenomena for electrochemically deposited thin film by cyclic voltammetry and chronoamperometry.

A potential of 450 mV (100 mV negative than the Nernst potential) was selected for the deposition procedure for all the conditions. The sole impact of sonication was experimented before the study of the coupling effect and was found to favor nucleation ahead of growth. The evidence of secondary nucleation in ultrasonic condition was also observed. The thickness of films lies in the range of 400-500 nm. The phases of the deposits are confirmed by the XRD analysis. The nucleation population density got increased from a low value to high value of acid concentrations. Comparison with the theoretical models, it is apparent that copper follows progressive nucleation mode in increasing acid concentration. Hydrogen evolution was also imperative at increasing acid concentrations, however, ultrasound capable of degassing produced hydrogen free adherent surfaces. The facts are also confirmed by the morphological analysis by SEM and AFM. The same trend is observed for the films with low temperatures. Among all the depositions copper films at – 4 °C is the smoothest. Increasing metal ion concentrations produces finer and harder deposits. Films are rougher at 0.1 M as compared to that of 0.025 M. The grains are found to vary from 400 nm to 50 nm at various conditions with the average roughness factors from 300 nm to 14 nm.

INTRODUCTION

Most materials used in advanced microelectronic devices are in thin film form. Thin films are also essential components of microelectromechanical systems (MEMS). Besides the microelectronics and MEMS industries, thin films and coatings are also extensively used as wear resistant coatings on cutting tools, protective coatings in data storage devices, and thermal barrier coatings on turbine blades. Copper films and lines are used as interconnections on printed circuit boards, systems in packages and semiconductor devices. Electrodeposition is one of the methods of obtaining metallic films and lines with adequate thickness, porosity-free structure and good adhesion. Electrodeposition as a means of materials synthesis offers the advantages of low processing temperatures, control of film thickness, and deposit onto complex shapes, low capital investment and the production of non-equilibrium materials that cannot be accessed by traditional processes. Nucleation and growth processes in electrochemical metal deposition monitor important microstructural features of the substrate i.e. grain size, crystallographic texture, dislocation density and internal stresses. These in turn determine the physical, chemical, electric and magnetic properties of metal deposit. Electrocrystalisation occurs either by the build-up of existing crystals or by the formation of new ones. These two processes are in computation with each other and are influenced by the different operating parameters such as bath composition, pH, bath temperature, overpotential, bath additives etc. The two key mechanisms that have been identified as the measure of rate determining steps for ultra-fine crystal formation are charge transfer at the electrode surface and surface diffusion of adions on the crystal surface. For a supersaturated solution phase the former dominates the control of rate of the reaction whereas the reverse is true for a depleting ion concentration near an electrode.

Around 1950 a new method of synthesis appeared associating electrodeposition and ultrasound but the current term of ‘‘sonoelectrochemistry’’ was employed several decades later. Use of ultrasound is in fact interesting because, if the power density is sufficient, mechanical energy resulting from sonotrode causes a cavitation in the liquid, i.e. production and implosion of microbubbles, giving rise to particular electrochemical reactions. Moreover ultrasound permits the replenishment of the double layer with metal cations and acceleration of mass transport leading to enhanced reaction rates. Ultrasound keeps the electrode surface clean and improves

mass transport such that uniform electrode reaction occurs across the area of a centimetre-scale electrode, with consequently greater reaction velocity at the electrodes.

The present work has been carried out with an aim to understand nucleation, growth mechanism and the effect of different operating parameters on the morphology and properties of sonoelectrochemically deposited copper thin film. The copper thin films have been prepared at varying acid concentrations, temperatures and metal ion concentrations in under insonation.

Chapter 1 cover the literature underlying the basic principles thin film nucleation and growth. Different approaches for thin film preparation have been covered briefly with a wide spectrum for electrodeposition. Fundamentals of electrochemical nucleation and growth with some well established models have been dealt with great details. The various aspects of sonoelectrochemistry have been covered. And the chapter concludes with the basic aims of the project work.

Chapter 2 deals with methods & materials and the various characterization techniques used to synthesize and characterize the copper thin films. The synthesis and electrochemical analysis portions include the description of cyclic voltammetry and chronoamperometry techniques in detail. The phase analysis study was described by the understanding of X-ray diffraction (XRD) technique. Topographical structural characterization is understood by the scanning electron microscope (SEM) and atomic force microscope (AFM) methods. Finally an attempt has been made to study the hardness properties of the thin films by nanoindentation.

Results and discussion are covered in chapter 3. Cyclic voltammetry for copper have been carried out for the conditions with and without ultrasound. The details are used for the final synthesis of films at a single potential step at various conditions. The chronoamperometric current transients are explained and analyzed. XRD has been properly used for the phase identification. The surface morphologies are characterized by SEM and AFM. The analysis confirms the nano range deposit with decreasing temperature, increasing acid concentration and copper concentration. Hardness of thin films was measured by nanoindentation tests. The result shows values corresponding to the obtained results from the characterization part.

Conclusions enlist the detailed results obtained from chapter 3. Finally a list of references has been included referred for the preparation of the thesis. However, the work needs further amplification to explore the electrochemistry in presence of ultrasound with various parameters.

Chapter 1

Literature Survey

Literature Survey

1.1 Thin film

Thin film is microscopically thin layer of material that is as grown from the substrate or deposited onto a metal, ceramic, semiconductor or plastic substrate. We can also define thin film, as a layer of material deposited onto substrates to achieve properties unattainable or not easily attainable in the substrates alone (a larger surface to volume ratio), with one dimension much smaller than the other two. Thin film technology has been developed primarily for the need of integrated circuit industry. Typically less than one micron thick, thin films can be conductive or dielectric (non-conductive) and are capable of myriad applications.

In thin films, deviations from the properties of the corresponding bulk materials arise because of their small thickness, large surface-to-volume ratio, and unique physical structure which is a direct consequence of the growth process. Apart from the conventional bulk properties, some of the phenomena arising as a natural consequence of small thickness are optical interference , electronic tunneling through an insulating layer , high resistivity and low temperature coefficient of resistance , increase in critical magnetic field and critical temperature of superconductor , the Josephson effect, and planar magnetization. The high surface to volume ratio of thin films due to their small thickness and microstructure can influence a number of phenomena such as gas adsorption, diffusion, and catalytic activity. Similarly enhancement of superconducting transition temperature, corrosion resistance, hardness, thermopower and optical absorption arises in thin films of certain materials having metastable disordered structures [1].

1.2 Properties and applications of thin film

Thin films show different properties than the bulk materials because of many factors such as smaller size of the crystallites and in particular many crystallographic defects such as dislocations, vacancies, stacking faults, grain boundaries and twins. Accordingly the properties upgradations with their possible uses in various contexts may be underlined briefly as followed in the table.

Table 1.1 Properties and applications of thin film

Thin film property-category	Applications
Optical	Reflective/antireflective coatings
	Interference filters
	Decoration (color, luster)
	Compact discs (CDs)
Electrical	Insulation
	Conduction
	Semiconductor devices
Magnetic	Memory discs
Chemical	Barriers to diffusion or alloying
	Protection against oxidation or corrosion
	Gas/liquid sensors
Mechanical	Tribological (wear-resistant) coatings
	Hardness
	Adhesion
	Micromechanics

1.3 Thin Film Technology

There are a myriad of sciences involved in the study of thin films and still are under debate. This may not be possible to bring them together, however the technology behind the topic has ample scope to link all of them at a place. Hence this section will be devoted to the process, the modes, and the deposition techniques of the ever demanding category in materials technology. And a special part will be dedicated for the thermodynamics and kinetics of the phase formation for the nucleation and growth of the films. As pointed earlier the films can be grown from the substrate either physical or chemical means or foreign materials can be deposited on the substrate. Now the next part to be covered should be the mode of the films (depends upon the chemical and physical interaction of substrate and deposit) to be fabricated, and finally the techniques of deposition.

1.4 Modes of growth of Thin Films.

Monolayer appearance and growth is essentially the formation of a continuous, complete, and single layer of atoms. Many experimental observations revealed that there are three basic mechanisms governing the formation of thin films. In general film formation can be the result of any of the following three modes

1. Frank-Van der Merwe Growth (Layer by Layer Growth),
2. Volmer-Weber Growth (3D Nucleation, Island Growth)
3. Stranski-Krastanov (SK Growth, Mixed mode)

Which mechanism actually dominates in the formation of a multilayer depends on the strength of interaction between the atoms of the growing film and between the atoms of the film and the substrate. Figure 1.1 illustrates these three basic modes of initial nucleation in the film growth.

1.4.1 Frank-Van der Merwe Growth (Layer by Layer Mode)

In this growth mode, initially one monolayer thick islands of atoms form and then they intergrow to form a single, continuous layer before significant clusters are developed on the next film layer [2]. This happens when the atoms are more strongly bound to the substrate than to each other. This growth mode is observed in the case of adsorbed gases, such as several rare gases on graphite and on several metals, in some metal-metal systems, and in semiconductor growth on semiconductors [3]. The driving force of this mode of growth is the reduction in the total surface energy i.e.

$$\gamma_I + \gamma_F \leq \gamma_S \qquad (1.1)$$

where γ_I, γ_F and γ_S the interface, film and substrate surface energies respectively. For a case of deposition of a film on a clean surface of the same material, $\gamma_I = 0$ and $\gamma_F = \gamma_S$, and equation (1.1) is satisfied. For deposition of films on dissimilar substrates, the growth modes is favoured strongly for low misfits (i.e. low γ_I), in the presence of strong bonding between the film and the substrate (or negative heat of mixing) which implies low interfacial energy, low film surface energy and high substrate surface energy.

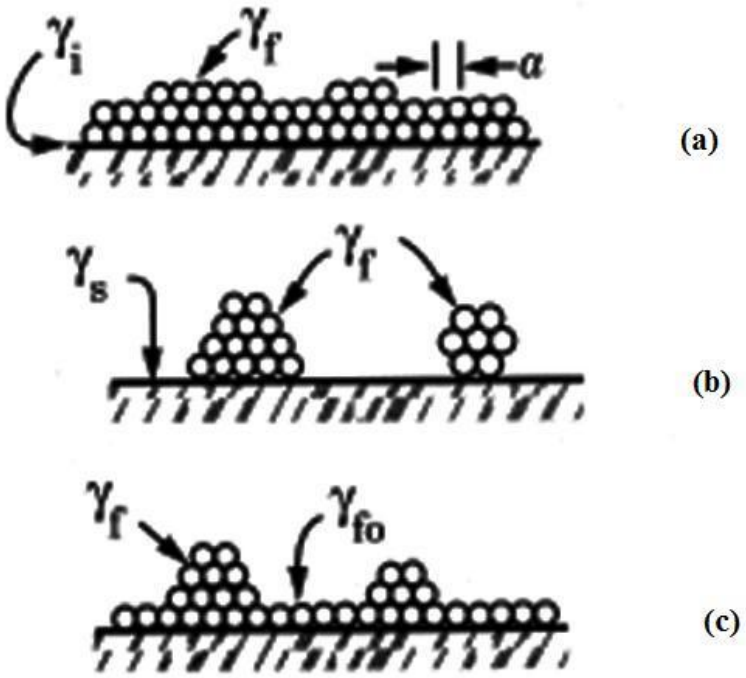

Figure 1.1: Film growth modes: (a) Layer by Layer (Frank-Van der Merwe); (b) Island (Volmer-Weber); (c) Stranski-Krastanov

It is also necessary to take elastic strain energy into account which increases with number of monolayers. This is done by replacing γ_I with γ_{IN} where N is the number of monolayers. After the initial formation of monolayer, subsequent monolayer grows on the top of each other until film thickness is reached. At this stage dislocations begin to form and result in the commencement of strain relief. This phenomenon progresses as the film growth continues [2].

1.4.2 Volmer-Weber Growth (Island Mode)

In the island, or Volmer-Weber mode, small clusters are nucleated directly on the substrate surface and then grow into islands of the condensed phase. This happens when the atoms (or molecules) of the deposit are more strongly bound to each other than to the substrate. This mode is displayed by many systems of metals growing on insulators, including many metals on alkali halides, graphite and other layer compounds such as mica [3].

Volmer-Weber growth mode prevails in the circumstances when the energy reduction criterion as shown in equation (1.1) is not followed i.e.

$$\gamma_I + \gamma_F > \gamma_S \qquad (1.2)$$

The nucleation of 3-D nuclei takes place either by surface diffusion or by direct impingement of atoms, often at active sites such as crystal defects, atomic step or impurities. These sites act as a means for reducing the activation energy for nucleation or bonding of the nuclei to the substrate. The nucleation of this type can be understood well by classical nucleation theory. According to these theories considering the capillarity model, a stable nucleus is of radius more than a 'critical radius' to fulfill the free energy criterion which is given by the following equation

$$\Delta G = r^2(a_1\gamma_F + a_2\gamma_I - a_2\gamma_s) + a_3 r^3 \Delta G_V \qquad (1.3)$$

where $a_1 r^2$, $a_2 r^2$and $a_3 r^3$ are the area of nuclei exposed to vapor, contact area between substrate and nuclei, and volume of nuclei respectively, and a's are geometric constants. ΔG_V is the volume free energy change upon formation of a nucleus and is negative in sign and it is directly related to the substrate temperature and the deposition rate. Nuclei having their radius less than the value at which ΔG is maximum will spontaneously decompose or evaporate since that is the direction of reduction of free energy. So for a stable nucleus to form, its radius should be greater than a critical radius,r^* at which $d(\Delta G)/dr$ changes it sign from positive to negative. The critical radius is calculated by differentiating the equation (1.3) w.r.t. r and the derivative,$d(\Delta G)/dr$ is equal to 0, and can be written as

$$r^* = \frac{[-2(a_1\gamma_F + a_2\gamma_I - a_2\gamma_s)]}{[3a_3\Delta G_V\ ]} \qquad (1.4)$$

The formation of nuclei of radius greater than a critical radius occurs until further nucleation is not possible as the energy situation of growth becomes more favorable and growth of existing nuclei takes place by the addition of more atoms. Strain relief can take place at the interface by generation of misfit dislocations at the interface either before the islands' coalescence or after, depending upon the degree of pseudomorphism (pseudomorphism is the modification in the lattice spacing of the epitaxial deposit in the interface plane to match that of the substrate). Then the coalescence of islands may be either by selective deposition of atoms at some preferential

sites on the existing islands due to minimization of total surface energy or by liquid like coalescence of islands which is attributed to fast diffusion of atoms on the island surfaces leading to formation of a compound island whose shape is similar to that of two islands before coalescence. In practice, increasing the deposition rate or decreasing the substrate temperature enhances this kind of nucleation. Temperature additionally controls the surface diffusion of the atoms [2].

1.4.3 Stranski-Krastanov Growth (Mixed mode)

In this kind of growth mode, the growth changes from monolayer to island after formation of one or two monolayers. This is believed to happen because of stress increase and thus strain relief after the formation of few monolayers due to mismatch in the lattice spacings. Normally, this growth mode tends to occur when the lattice misfit is more than about 2% and the contribution due to strain energy is in equation (1.1) is larger than those from surface energies [2]. Apart from these there are many possible reasons for this mode to occur, and almost any factor which disturbs the monotonic decrease in binding energy, characteristic of layer growth, may be the cause. For example, the lattice parameter of, or symmetry of, or molecule orientation in, the intermediate layer may not be able to be continued into the bulk crystal of the deposit. These results in a high free energy of the deposit-intermediate-layer interface which favors subsequent island formation. There are many examples of its occurrence in metal-metal, metal-semiconductor, gas-metal and gas-layer compound systems [3]. To improve the quality of epitaxy, 3-D type of growth mode should be avoided or suppressed as it leads to the formation of defects such as twins, stacking faults and increased roughness in the films [2].

1.5 Deposition techniques of thin films

After the discussion of the modes of film nucleation and growth, this section is devoted to the methods/techniques by which films are primarily deposited. The thin film process comprises three elementary stages including decomposition, transport, and nucleation and growth mechanisms. Figure 1.2 shows the flow chart of the thin film process, where starting materials is successively modified to the resulting films. In the first stage, starting materials in the form of gas, liquid or solid are decomposed into various fragments of neutrals or ions in the form of atoms, molecules, clusters or powders by the external powers of plasma, laser, ion, microwave

and thermal energies. The decomposed fragments thus formed will travel through the medium of gas or liquid and approach to the substrate. This phase is referred to as the transport stage in the thin film process. The chemical reaction between the transport medium and the decomposed fragments is also important in the reactive process of thin film formation. The decomposed fragments land on the substrate for nucleation and growth, which result in the formation of functional films.

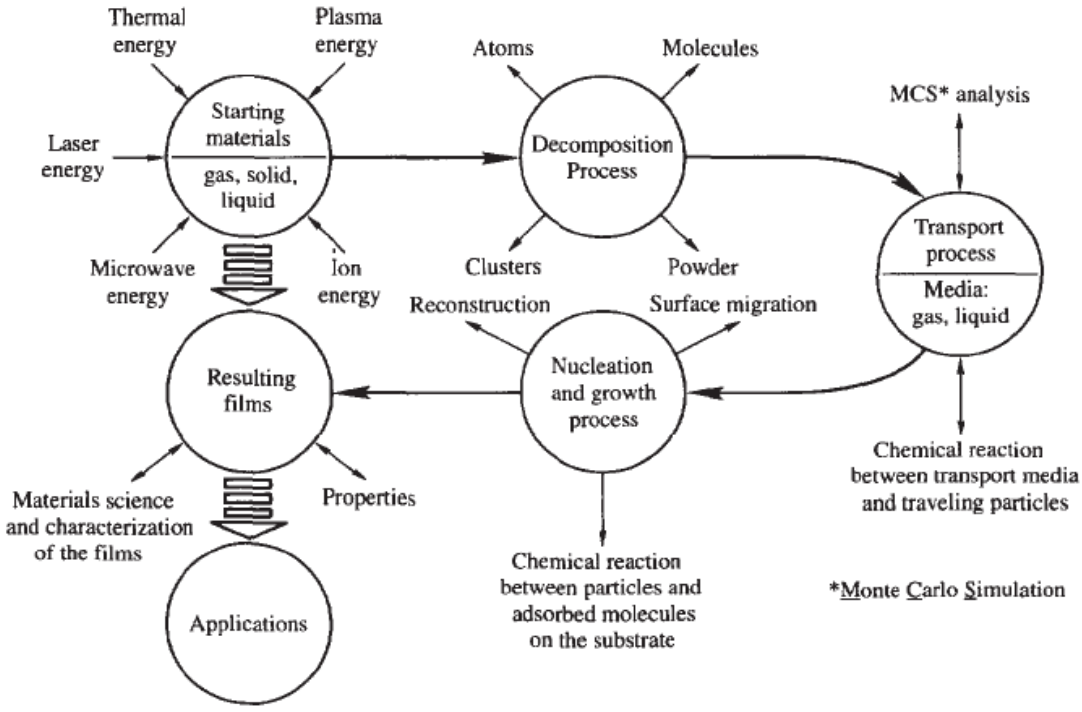

Figure 1.2: Flow chart of thin film process

Thin film properties are strongly influenced at this final stage, because the energy of the decomposed fragments is dissipated in the very shallow surface region of the substrate. This dissipation of the energy of the decomposed fragments may enhance the surface migration of ad atoms, chemical reaction between landing fragments and adsorbed molecules, and finally reconstruction into the structures of the resulting films [4]. Deposition techniques fall into two broad categories, depending on whether the process is primarily chemical or physical. Physical deposition uses mechanical or thermodynamic means to produce a thin film of solid. An everyday example is the formation of frost. Since most engineering materials are held together by relatively high energies, and chemical reactions are not used to store these energies,

commercial physical deposition systems tend to require a low-pressure vapor environment to function properly; most can be classified as Physical vapor deposition or PVD. In chemical type of process, fluid precursor undergoes a chemical change at a solid surface, leaving a solid layer. An everyday example is the formation of soot on a cool object when it is placed inside a flame. Since the fluid surrounds the solid object, deposition happens on every surface, with little regard to direction; thin films from chemical deposition techniques tend to be conformal, rather than directional. Apart from the above two basic formation processes there can be special category type of techniques i.e. molecular beam epitaxy (MBE), Langmuir-Blodgett films. Here as a part of the thesis the electrochemical deposition technique will be described in detail.

1.5.1 Electrochemical Deposition

Electrochemical deposition deals with the synthesis of solid films from dissolved species by alteration of their oxidation states using electricity. Not only pure metals can be prepared by electrochemical deposition but also compounds like oxides and phosphides can be easily fabricated. Important applications within the electronics industry are the deposition of copper interconnects in integrated circuits and the deposition of thin film magnetic materials, e.g. CoNiFe alloys. It has also a widespread use in nanotechnology since it can be used to fill three-dimensional features at room temperature with good control of thickness and morphology. Electrodeposition has many advantages over other processing techniques including [5, 6]:

- It provides a cost-effective and nonequipment-intensive method for the preparation of materials (metals, alloys, compositionally modulated alloys and composites) either as coatings or as freestanding objects even in complex shapes (foils, wires, electroforms).
- The low processing temperature (around room temperature) minimizes interdiffusion or chemical reaction.
- The film thickness can be accurately controlled by monitoring the consumed charge.
- Composition and defect chemistry can be controlled by electrical and fluid-dynamic means.
- Deposition rates of the order of several tens of microns per hour can be routinely achieved.
- The capability of single-step production and the ability to produce fully dense materials, free of extraneous porosity.

- Electrodeposition can be used in systems that do not lend themselves to vacuum deposition.
- Electrodeposition is a feasible technique for the production of thin multilayered materials.
- Coating produced by electrodeposition display the same coherence and layer thickness uniformity as those of composition-modulated alloys produced by vacuum evaporation or sputter deposition.

Fundamental aspects of electrochemical deposition include the heterogeneous electron transfer step between the electrode and the electroactive species present in the solution as well as the transition of the discharged metal atoms into the crystalline state. Electrochemical deposition of metals and metal oxides typically proceeds by oxidation or reduction of species in a solution. The standard electrode potential for an electrochemical reaction is the potential where the rate of the reduction and the oxidation reactions are equal at standard conditions of concentrations, pressure and temperature. The Nernst equation relates the standard electrode potential E^0 to the electrode potential E:

$$E = E^0 + \frac{RT}{nF} ln \frac{\{ox\}}{\{red\}} \qquad (1.5)$$

Where R is denotes the standard gas constant (8.314510 J-$K^{-1}mol^{-1}$), T the absolute temperature in Kelvin, n the number of electrons transferred and F the Faraday's constant (96485.309 $C.mol^{-1}$). The potential also depends on the ratio of natural logarithm of the activities of the oxidized and reduced species.

The electrolysis of species can be performed using a constant current forced through the electrochemical cell, while the electric potential is monitored. Alternatively, a desired potential can be chosen, which is then maintained by the instrument while the necessary current used to maintain that potential is monitored [7].

1.5.1.1 Deposition of Metals

The reductive electrochemical deposition of metals from aqueous solutions is a well-established field. Hence electro-crystallization not only represents an interesting case of phase formation and crystal growth but is also a powerful method for various technological applications because the driving force of the process can be easily controlled by the current

density and the electrode potential. The optimum current density for the deposition of compact coatings is generally that corresponding to the end of the Tafel linearity range, as the nucleation rate increases with more negative potentials but mass-transport limitations causes irregular growth. Nucleation is a very important process in metal deposition [7]. On one hand, the competition between growth and nucleation determines the granularity of the deposit. The higher the nucleation rate during deposition, the finer are the crystal grains of the deposit. On the other hand, the forms of the growing crystals determine the general appearance and structure of the deposit. With a higher growth rate of the crystal grains normal to the substrate surface, for instance, a fibrous structure of the deposit is obtained. Or, with large developed crystal faces parallel to the substrate a brightening effect can be achieved [8]. Accordingly the nucleation and growth studies are worthy of being experimented. Here we do represent a brief approach to the above phenomenal in an electrochemical context.

1.5.1.2 Electrochemical nucleation and growth: The concept of supersaturation

In order to initiate either the growth of the bulk crystal or a process of nucleus formation on the inert foreign substrate it is necessary to supersaturate the parent phase, the electrolyte solution. This means to increase its electrochemical potential to a value μ_s larger than that of the bulk new phase, the metal crystal ($\mu_s > \mu_{c,\infty}$). Then it is the difference $\Delta\mu = \mu_s - \mu_{c,\infty} > 0$, which defines the electrochemical supersaturation.

In the opposite case, when $\mu_s < \mu_{c,\infty}$, the difference $\mu_s - \mu_{c,\infty} < 0$ defines the electrochemical undersaturation, which, if applied, would cause the electrochemical dissolution of the bulk crystal.

The general formula for $\Delta\mu$ is : $\Delta\mu = ze\eta$ (1.6)

Where η is the cathodic overpotential defined either as

$$\eta = E_\infty - E \tag{1.7}$$

or as

$$\eta = \frac{kT}{ze} ln \frac{a_s}{a_{s,\infty}} \tag{1.8}$$

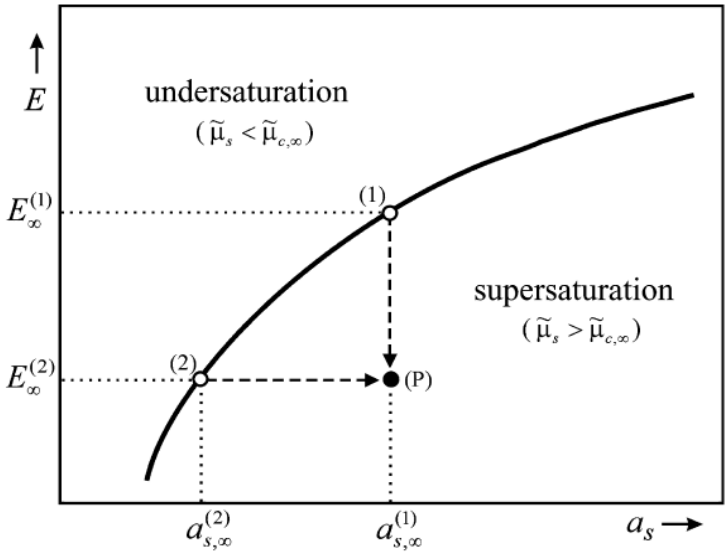

Figure 1.3: Schematic Potential-Activity (E-a_s) diagram for the equilibrium of a bulk metal crystal with its own ionic solution

Where E_∞ is the equilibrium potential of a bulk metal crystal dipped in a solution of its ion with activity $a_{s,\infty}$. The supersaturation may initiate both the process of nucleus formation on the foreign substrate and the growth of the bulk metal crystal, depending on which phase is switched on as a working electrode.

1.5.1.3 The Thermodynamic Work for Nucleus Formation

The electrode potential is directly connected to the energy change of the electrode process through the relationship:

$$\Delta G^0 = -nFE^0 \qquad (1.9)$$

When the electrode potential is made more negative in relation to the standard reduction potential for an electrochemical reaction, the reduction current increases because the rate of electron transfer of the reduction increases. In the electron transfer controlled potential region, there is a linear relationship between the potential and the logarithm of the deposition current known as the Tafel linearity. However, the current can also be limited by other factors such as mass transfer, preceding chemical steps and crystallization processes.

The formation of an n-atomic nucleus of the new phase requires one to overcome a thermodynamic barrier *ΔG(n)* called nucleation work and expressed by the general formula.

$$\Delta G(n) = -n\Delta\mu + \Phi(n) \qquad (1.10)$$

Here *Φ(n)* takes into consideration the total energy excess due to the creation of new interfaces when a nucleus appears on the electrode surface.

1.5.1.4 Classical Nucleation Theory

In the particular case of sufficiently large clusters the number of atoms 'n' can be considered as a continuous variable and the quantity $\Phi(n)$ could be expressed by means of the specific free surface, interfacial and line energies in the system nucleus–electrolyte–working electrode. In that case *ΔG(n)* is a differentiable function and the condition for an extreme $[d\Phi(n)/dn]_{n=n_c} = 0]$ yields

$$\Delta\mu = \left[\frac{d\Phi(n)}{dn}\right]_{n=n_c} \qquad (1.11)$$

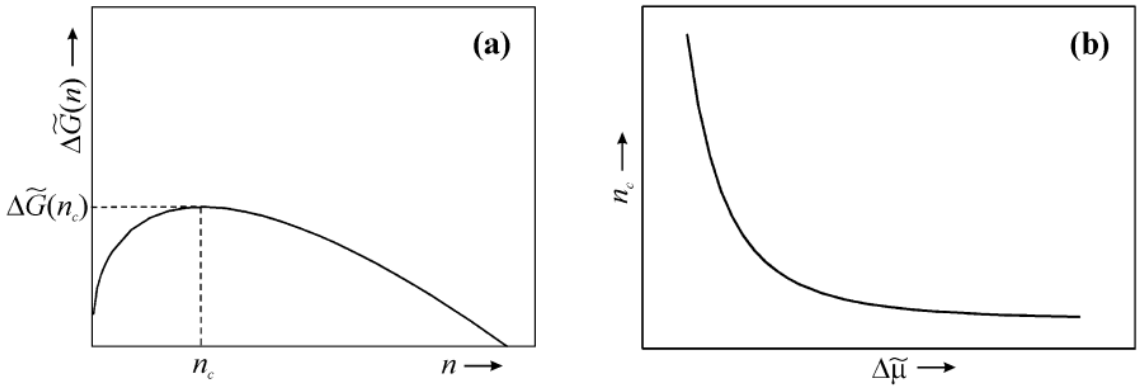

Figure 1.4: (a) dependence of the nucleation work ΔG(n) on the cluster size n, and (b) dependence of the critical nucleus size n_c on the supersaturation Δμ according to the classical nucleation theory

Equation (1.11) represents a general expression for the Gibbs–Thomson equation giving us the interrelation between the supersaturation $\Delta\mu$ and the size n_c of the so-called critical nucleus, which stays in unstable equilibrium with the supersaturated parent phase.

The inspection of the theoretical formula for the nucleation work shows that the $\Delta G(n)$ versus n relationship displays a maximum at $n = n_c$, the values of $\Delta G(n_c)$, n_c and $\Delta\mu$ being interrelated according to

$$\Delta G\left(n_{c,3D}\right) = \frac{1}{3}\Phi\left(n_{c,3D}\right) = \frac{1}{2}n_{c,3D}\Delta\mu \qquad (1.12)$$

when 3D cluster form on a foreign substrate and according to

$$\Delta G\left(n_{c,2D}\right) = \frac{1}{2}\Phi\left(n_{c,2D}\right) = n_{c,2D}\Delta\mu \qquad (1.13)$$

and

$$\Delta G\left(n^*_{c,2D}\right) = \frac{1}{2}\Phi\left(n^*_{c,2D}\right) = n^*_{c,2D}\mu_{2D} \qquad (1.14)$$

when 2D clusters form on a native or on a foreign substrate, respectively.

1.5.1.5 Atomistic Nucleation Theory

In the case of very small clusters the size n is a discrete variable and the macroscopic classical theory cannot be applied. Therefore the process of nucleus formation is described by means of atomistic considerations making use of the general formula for the nucleation work, equation (1.10). The main result of the atomistic treatment is that the $\Delta G(n)$ vs. n relationship is not a fluent curve but displays minima and maxima, depending on the structure and energy state of the cluster (Fig.1.5(a)). The highest maximum at a given supersaturation corresponds to the critical nucleus size. The discrete change in the size of the clusters at small dimensions also affects the $n_c(\Delta\mu)$ relationship. As seen from Fig.1.5 (b), in this case there corresponds to each critical nucleus a supersaturation interval and not a fixed value of $\Delta\mu$ as predicted by the Gibbs–Thomson equation. These special properties of small clusters influence strongly the process of

phase formation during electrocrystallization and have to be taken into consideration, particularly when interpreting experimental data for electrochemical nucleation on a foreign substrate. In that case the size of the critical nuclei does not exceed several atoms.

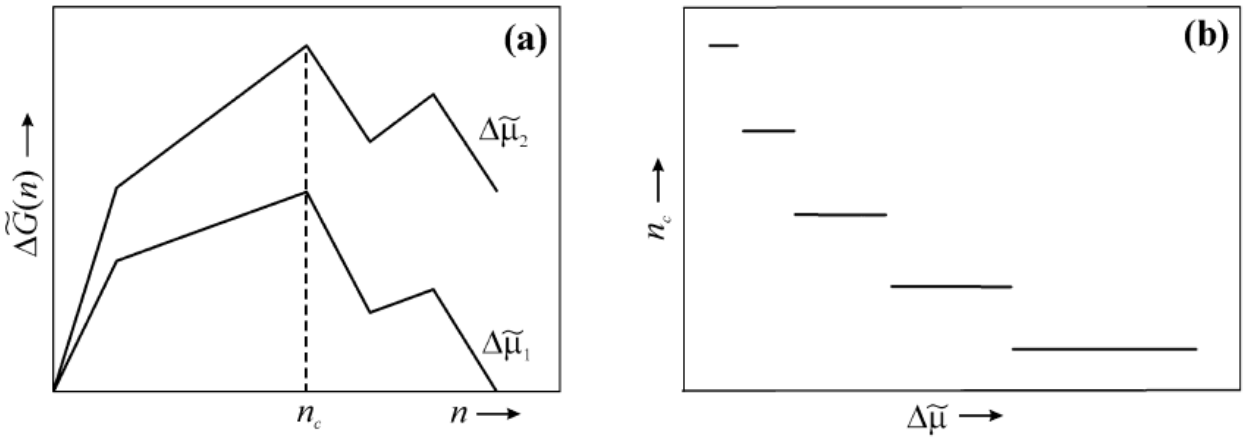

Figure 1.5: (a) dependence of the nucleation work ΔG(n) on the cluster size n, and (b) dependence of the critical nucleus size n_c on the supersaturation Δμ according to the atomistic nucleation theory.

1.5.1.6 Kinetics of Nucleus Formation in Electrocrystallization

The nucleation work $\Delta G(n_c)$ is a measure of the thermodynamic barrier, which has to be overcome in order to transform n_c ions from the electrolyte solution into an n_c-atomic nucleus of the new solid or liquid phase on the electrode surface.

The existence of an energy barrier makes the nucleation a probability process, with a rate J (nuclei/cm^{-2} s^{-1}) given by the probability for their formation.

The general theoretical formula for J_0

$$J_0 = Z_0 W \lambda^{-1} \exp\left[-\frac{\Delta G(n_c)}{kT}\right] \qquad (1.15)$$

where Z_0/cm^{-2} is the number density of active sites on the substrate, W/s^{-1} is the frequency of attachment of single atoms to the critical nucleus and λ^{-1} is a nondimensional quantity accounting for the difference between the quasi-equilibrium and the stationary number of critical nuclei. In the macroscopic classical nucleation theory λ^{-1} is given as $\lambda^{-1} = \left[\frac{\Delta G(n_c)}{3\pi n_c^2 kT}\right]^{1/2}$ and is

called “Zeldovich factor”. It tends to unity at high supersaturations and/or very active substrates, when the critical nuclei are very small and their size remains constant over wide supersaturation intervals. For this typical case of electrochemical phase formation, particularly on foreign substrates, we shall reveal the overpotential and the concentration dependence of the stationary nucleation rate in terms of the atomistic theory of electrochemical phase formation. In this case the quantity W is given by

$$W = k_v \exp\left(-\frac{U}{kT}\right)\exp\left(-\frac{\alpha zeE}{kT}\right) \qquad (1.16)$$

where k_v is a frequency factor, c is the concentration of metal ions, α is the charge transfer coefficient and U is the energy barrier to transfer of an ion from the electrolyte to the critical nucleus at an electrode potential E = 0. This formula for W is suitable when the supersaturation Δμ is varied by changing the concentration of metal ions at a constant electrode potential E.
The size n_c of the critical nucleus can be determined from an experimental $J_0(c)$ relationship obtained at E = const according to

$$n_c = \frac{dlnJ_0}{dlnc} - 1 \qquad (1.17)$$

In the case when the supersaturation is varied by varying the electrode potential E at a constant concentration c_∞, the size n_c of the critical nucleus can be determined from an experimental $J_0(\eta)$ relationship obtained at $c = c_\infty$ according to

$$n_c = \frac{kT}{ze}\frac{dlnJ_0}{d\eta} - \alpha \qquad (1.18)$$

where η is the cathodic overpotential, [9].
Additives are commonly used in plating baths to improve the adhesion and material properties of the metal deposits. Leveling agents are organic molecules that adsorb on the surface and accelerate the rate of the deposition within trenches, thus enabling depositions of smooth and bright deposits [7].

1.5.1.7 Thermodynamics (diffusion) versus Kinetic control

In an electrochemical cell the current forced through the solution is carried by ions. The consumption of species during the reduction at the working electrode gives rise to a concentration gradient in the solution outside the electrode surface. The random motion of the species by which this concentration difference is equalized is called diffusion. In an unstirred solution the diffusion layer thickness extends into the solution until vibration and thermal movement start to contribute to the mass transport. The current is generally limited either by the mass transport of species towards the electrode or by the kinetics of the electrode reaction. On the other hand, determinations of the diffusion coefficient of species in the solution by electrochemical methods require that the kinetics of the electrode reaction does not limit the current.

When an electrochemical experiment is performed using a constant current, the potential shifts to the value required to maintain that current. Under conditions of mass transfer control (i.e. when the kinetics of the electrode reaction does not limit the current), the potential shifts when the concentration of electroactive species at the electrode surface is reduced to zero. The time needed for this depletion of the species, the transition time τ, is given by the Sand equation:

$$\tau^{1/2} = \frac{nF(\pi D)^{1/2} C^*}{2I} \qquad (1.19)$$

where I is the current (in mA), C^* is the bulk concentration (in mol·cm^{-3}), and D is the diffusion coefficient expressed in cm^2·s^{-1}. For Cu^{2+} in aqueous solution, D = 3.6×10^{-6} cm^2·s^{-1}. [7]

1.5.1.8 Electrochemistry towards nanofabrication:

There is quiet revolution going on, and its name is nanotechnology. Without much fanfare, a host of innovations are coming our way. Use of electrochemistry, the solid/liquid interface science, in nanoscience and nanotechnology may range from nanosystems, to nanosynthesis, to nano characterization. The characteristic reaction may be ion transfer reaction (ITR) or electron transfer reaction (ETR).The nanoscale electrochemistry covering from metallic and semiconductor based nanoparticles, nanoarrays, nanotubes, nanopits [10], to self assembled molecule monolayers i.e. bioelectrochemical systems with redox metalloprotein or DNA based

molecules [11], has began to unravel the complexities of these systems. Electrochemistry is a suitable method for coupling particles activity to external circuitry. It has been successfully used in investigating the effects and kinetics of charge transfer [12] at Q-dots using scanning electrochemical microscopy (SECM), by controlled transport reactions. Electrocrystallization processes occurring at electrochemical solid/liquid interfaces have for a long time attracted the interest of many researchers from both fundamental and applied viewpoints. Electrocrystallization not only represents an interesting case of phase formation and crystal growth but is also a powerful method for various technological applications because the driving force of the process can be easily controlled by the current density and the electrode potential [13]. Over the past decade, electrodeposited nanostrutures have advanced rapidly to commercial application because of the following factors, i) an established industrial infrastructure, ii) relatively low cost of application where by nanomaterials can be produced by simple modification of bath chemistry and electrical; parameters used in current plating and electroforming operations, iii) the capability in a single step process to produce metals, alloys and metal-matrix composites in various forms, iv) the ability to produce fully dense nanostructures free of extraneous porosity. Important processing parameters include bath composition, pH, temperature, overpotential, bath additives, substrate types etc.

1.5.1.9 Factors affecting nucleation and growth phenomena at the electrode surface:

In view of the industrial importance of the electrodeposition of metals, the influence of various factors on the physical appearance of the deposits has been the subject of much investigation. It is generally agreed that electrodeposited metals are crystalline, and the external appearance depends mainly on the rate at which the crystals grow and on the rate of the formation of fresh nuclei. If the conditions are such as to favor the rapid formation of crystal nuclei, the deposit will be fine grained; if the tendency is for the nuclei to grow rapidly, however, relatively large crystals will form and the deposit becomes rough in appearance [14]. Hence the next part of the thesis will be describing the various factors affecting the appearance and growth of the deposits.

1.5.1.9.1 Current Density

At low current densities the discharge of ions occurs slowly, and so the rate of the growth of the nuclei should exceed the rate at which new ones form; the deposits obtained under these conditions should be coarsely crystalline. As the current density is raised the rate of formation of nuclei will be greater and the deposit will become finer-grained. At very high currents the solution in the vicinity of the cathode will be depleted in the ions required for discharge, and, as a result, the crystals will tend to grow outwards towards regions of higher concentration; the deposit then consists of "trees," nodules or protruding crystals. If the current density exceeds the limiting value for the given electrolyte, hydrogen will be evolved at the same time as the metal is deposited; bubble formation often interferes with crystal growth, and porous and spongy deposits may be obtained. The discharge of hydrogen ions frequently causes the solution in the vicinity of the cathode to become alkaline, with the consequent precipitation of hydrous oxides or basic salts; if these are included in the deposit, the latter will be fine-grained and dark in appearance. The above mentioned effects are readily observed by Ghasemi et.al. [15]

1.5.1.9.2 Deposition Potential

The constant potential is good to control the polarization and the deposition potential so that it can control the content of each element in compound and the current efficiency. It was found that deposition potential mostly affects the density of nuclei on the electrode substrate. However some researchers have also mentioned the unaffected nuclei number density with increased deposition potential [16].

1.5.1.9.3 Concentration of Electrolyte

The effects of the electrolyte concentration and of current density are to a great extent complementary by increasing the concentration or by agitating the solution, higher current densities can be used before coarse deposits are formed, or before hydrogen evolution occurs with its accompanying spongy or dark deposits. The influence of concentration on the rate of nucleus formation is uncertain; since increase of concentration tends to give firm, adherent deposits, some workers have expressed the opinion that the presence of the large number of ions in a concentrated solution favors the formation of fresh nuclei [16]. Certain experiments, however, indicate that the rate of formation of nuclei is actually decreased by increasing

concentration, but the improvement in the deposit is due to an increase in the rate of growth of crystals over the cathode surface, combined with a decrease in the rate of growth in a perpendicular direction. The results obtained by T. Mahalingam et al. do follow non-uniform and coarse grained morphology for Ni-P thin films with increasing NaH_2PO_2 concentration [17].

1.5.1.9.4 Temperature

The velocity (diffusion and migration) of the metal ions and inhibitor molecules are functions of the temperature. Increase in temperature usually increases concentration of metal in the cathode diffusion layer and may affect the cathode current efficiency of deposition of metals, particularly those deposited from complex ions. A high temperature causes an increased ion supply toward the cathode and the cathodic overpotential decreases. Thus increase of electrolyte temperature should decrease cathodic and anodic polarization [18]. Both the viscosity and the surface tension of the solution also decrease with increasing temperature. The energy barrier that the ions have to surmount for an adatom formation is an obvious function of temperature as mentioned in section 1.5.1.3. An increased energy for the nucleation process means a decreased rate of nuclei formation and a preferred growth of existing nuclei. The consequence is the formation of coarse grains. Small metal grains have high interface energy and a high tendency for the reduction of the interface energy by grain growth. Migration of atoms in the interface is a function of temperature [19, 20]. And decreasing temperature should increase the level of supersaturation. Hence, the activity of ions will increase and the critical nucleating condition will occur at low temperature. Hence temperature can affect the crystal growth by several ways, all of them predominantly resulting in a smaller crystal size at low temperatures [21].

1.5.1.9.5 Acid Concentration or pH

A study of the variation in the surface morphology with pH revealed that low pH values tend to favor the formation of smooth bright deposits. However medium pH values tend to enhance the rate of nucleation. Hardness value also tends to decline when the pH is increased [22]. The pH increases produces a shift of electrode potential towards more positive values within the cathodic range and more negative within the anodic range. The cathodic efficiency decreases with the increasing alkalinity of the solution beyond the 8.5 value [18]. Open circuit potential of the metal does not change with time; its value is dependent on the solution pH, i.e.

concentration of H+ ion, and becomes more negative as the pH increases in an acidic solution. Decreasing pH of the electrolyte led to the increase of hydrogen evolution reaction and hydrogen bubbles which cling to the surface and decrease the effective surface area of the metal reduction reaction. These could reduce the limiting current density. The crystallinity and grain size in the deposits decreased with the decrease of bulk pHs due to a high polarization [23]. Grujicic and Pesic were studied the nucleation behavior of copper at solution pH 1, 2, and 3 and they found that some of the grains at pH 2 are quite larger than at pH 1. At pH 3 the grain become elongated and less populated on the surface. Thus, pH increase was responsible for the grain hight increase, as well as the increase of irregularity of grain shapes, and the decrease of surface nuclei population density.

1.5.2 The experiment

For the evaluation of the nucleation and growth phenomena in different electrochemical systems several techniques have been developed. Most of them are based on the chronoamperometric current transients (CCTs) with a single voltage loop. Cyclic voltammetry is normally used to investigate the occurrence and progress of the phase formation. However it is the CCT technique to quantitatively study the two phases simultaneously. The most straightforward technique is the application of a voltage double pulse. The amplitude of the first pulse is chosen in the range of nucleation. According to the duration of the pulse one or several nuclei may be formed which are grown at a succeeding lower overpotential to a visible size [24, 25]. A second useful technique is to apply a short nucleation pulse and to record the following current transient in the region of growth. From the resulting *i-t* relation the number of nuclei can be evaluated. A number of approaches have been made to do the evaluations and are listed below:

1.6 Nucleation and Growth Theories

A nucleus, a cluster of atoms, is only stable if it exceeds a critical size. The growth of each individual nucleus is then determined by the rate of incorporation of new atoms, i.e. ion transfer and/or diffusion. As growth proceeds, there is overlap of the growth centers. In the case of pure ion transfer control, this corresponds to the physical coalescence of the growing nuclei. In the

case of diffusion control however, interference of the diffusion zones must be considered. And the theories corresponding to the calculations are:

1.6.1 Scharifker and Hills Theory

The early stages of electrochemical phase transformations are usually associated with two- or three-dimensional nucleation processes, the rate of which and hence the number of nuclei so formed, being strongly dependent on the overpotential. In many cases of electrodeposition reaction, notably in the deposition of metals from molten salts or aqueous solutions, the charge transfer step is found to be fast and the rate of growth of mature nuclei are well describe in terms of control by mass transfer of electrodepositing ions to the growing centers. Because of small size, the growth of nuclei would be described in terms of localized spherical diffusion [26].

The analysis of current time transient is an important technique for studying the kinetics of electrocrystallization. The form of the current transient is a typical characteristic of an electrochemical nucleation and growth process. All transient exhibit a similar behavior; these are illustrated by a rapid decrease in current at very short time, which corresponds to charging of the double layer. This is followed by an increase in current due to the isolated growth of all individual nuclei and the increasing number of these nuclei present on the electrode surface. During this stage, the transport of electroactive species to nuclei formed on the surface occurs through hemispherical diffusion zones developed around each individual nucleus. As these grow, the coalescence of neighboring diffusion zones with localized hemispherical nuclei gives increase to a current maximum, followed by a decaying current, related to planer electrode diffusion. These features are consistent with nucleation of 3D hemispherical clusters followed by diffusion limited growth. According to Sharifker and Hill, the rate law for growth of 3D islands during electrochemical deposition is dependent on the mechanism of nucleation and growth. Analysis of early stages of nucleation, leads to two limiting cases. The two limited models are instantaneous or progressive three-dimensional nucleation with hemispherical diffusion-controlled growth of nuclei [27]. Instantaneous nucleation corresponds to a slow growth of nuclei on a small number of active sites, all activated at the same time. In this case all active sites available on the electrode surface are occupied in a very short time period after applying overpotentials and then, the nuclei only grow. Therefore instantaneous nucleation occurs when the nucleation rate is very high. Progressive nucleation corresponds to a fast growth of nuclei on

many active sites, all activated during the course of electroreduction. In this case nuclei are continuously formed during the whole time period at which overpotential is applied. So progressive nucleation will occur when nucleation rate is low [28, 16].

Table 1.2: Important results of Sharifker and Hills theory

S. no.	Instantaneous nucleation	Progressive nucleation
1.	$t_m = \left(\frac{1.2564}{N\pi kD}\right)$	$t_m = \left(\frac{4.6733}{AN_\infty \pi k' D}\right)^{1/2}$
2.	$I_m = 0.6382\ zFDc(kN)^{1/2}$	$I_m = 0.4615\ zFD^{3/4}c(k' AN_\infty)^{1/4}$
3.	$I_m^2 t_m = 0.1629\ (zFc)^2 D$	$I_m^2 t_m = 0.2598\ (zFc)^2 D$
4.	$\frac{I^2}{I_m^2} = \frac{1.9542}{t/t_m}\left\{1 - \exp\left[-1.2564\left(\frac{t}{t_m}\right)\right]\right\}^2$	$\frac{I^2}{I_m^2} = \frac{1.2254}{t/t_m}\left\{1 - \exp\left[-2.3367\left(\frac{t}{t_m}\right)^2\right]\right\}^2$

The proposed equation of Sharifker and Hill for 3D nucleation and growth are given in table, where D is diffusion coefficient, c the bulk concentration, zF the molar charge of the electrodepositing species, N the total number of nuclei, N_∞ number density of active sites, I_m and t_m current and time coordinate of the peak and k and k' are numerical constant. k and k' can be defined as

$$k = \left(\frac{8\pi cM}{\rho}\right)^{1/2} \qquad (1.20)$$

and

$$k' = \frac{4}{3}\left(\frac{8\pi cM}{\rho}\right)^{1/2} \qquad (1.21)$$

where M and ρ are molecular weight and density of the deposited material respectively.
Experimental current transient can be presented in dimensionless form by plotting $(I/I_m)^2$ vs. t/t_m and comparing with the theoretical transients for instantaneous and progressive mechanism.

1.6.2 Scharifker and Mostany Theory

The model of Scharifker and Mostany ('SM model') essentially introduces the improvement that an a priori definition of k, $k=(8\pi cM/\rho)^{1/2}$ is used (in fact Scharifker and Hills' value for the instantaneous limit). To derive an expression for the total current, the current as a result of hemispherical diffusion towards a 'free' hemispherical nucleus is considered. As with the Scharifker and Hills ('SH') model, this is then 'projected' to give a problem in terms of circular diffusion zones, having time dependent radii. Scharifker and Mostany state that the appropriate time variable for the consideration of the size of the diffusion zone at time t is the time since the appearance of a nucleus, (t − u), where u is age of diffusion zone [29].

In the model of Scharifker and Mostany the current density to the whole electrode surface is

$$I = \left(\frac{zFD^{1/2}c}{\pi^{1/2}t^{1/2}}\right)(1 - \exp\{-N_0\pi kD[t - (1 - e^{-At})/A]\}) \qquad (1.22)$$

This expression can be presented in non-dimensional form by plotting $I^2/I_m{}^2$ vs. t/t_m, for different values of the dimensionless parameter $\alpha = N_0\pi kD/A$.

The current described by above equation passes through a maximum and therefore the current I_m and the time t_m corresponding to the maximum can be evaluated by equating the first derivative of above equation to 0. So we can write it as

$$\frac{I_m t_m^{1/2}}{a} = \frac{2x\left(1 - e^{-x/\alpha}\right)}{[1 + 2x(1 - e^{-x/\alpha})]} \qquad (1.23)$$

where $a = zFD^{1/2}c/\pi^{1/2}$, $x = N_0\pi kDt_m$, and $\alpha = N_0\pi kD/A$

We can use the appropriate values of x and α found above to construct a plot of $\frac{I_m t_m^2}{a}$ vs. logα.

From these two plots, it is possible to calculate both N_0 and A from the experimental values of I_m and t_m.

For instantaneous nucleation (α→0)

$$I = \left(a/t^{1/2}\right)[1 - \exp(-bt)] \qquad (1.24)$$

where $b = N_0 \pi k D$ and $t_m = 1.2564/b$. Introducing this value into equation (1.23) and rearranging

$$I_m t_m^{1/2}/a = 1 - \exp(-1.2564) \approx 0.7153 \qquad (1.25)$$

which is the limiting value of α→0 of $I_m t_m^{1/2}/a$.
For progressive nucleation (α→∞)

$$I = \left(a/t^{1/2}\right)[1 - \exp(-Abt^2/2)] \qquad (1.26)$$

and $t_m = (4.6733/Ab)^{1/2}$. Thus

$$I_m t_m^{1/2}/a = 1 - \exp(-2.3367) \approx 0.9034 \qquad (1.27)$$

this is the limiting value of α→∞
Then "instantaneous" and "progressive" nucleation can be considered as special, extreme cases of a more general phenomenon of heterogeneous nucleation on a finite number of active sites on the surface [30].

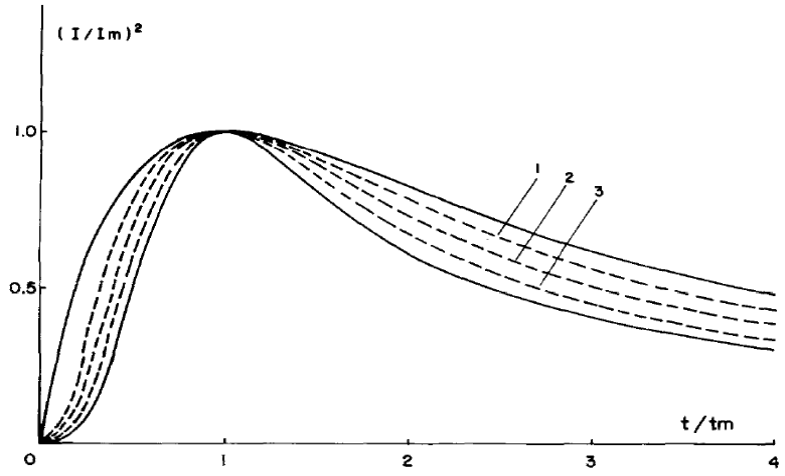

Figure 1.6 : Nondimensional plot of the transients for instantaneous (upper continuous curve) and progressive (lower continuous curve) nucleation.

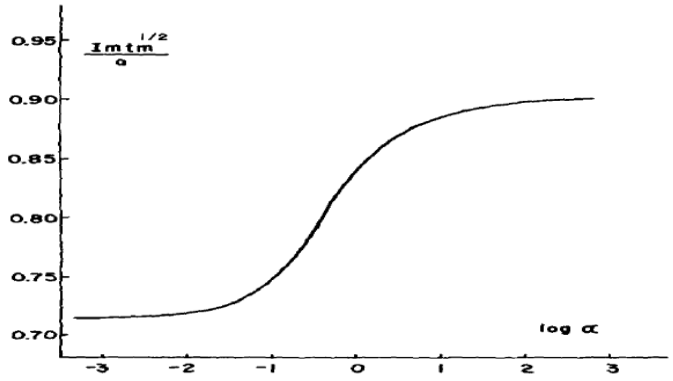

Figure 1.7: plot of $I_m t_m^{1/2}/a$ vs. log(α)

1.6.3 Sluyters-Rehbach, Wijenberg, Bosco, and Sluyters Theory

After initial delay or induction time, nucleation proceeds at a constant rate until it becomes limited by the available surface area or the available number of nucleation sites. Each nucleus - a cluster of atoms having a critical size - grows (mostly three-dimensionally) at a rate determined by the rate of incorporation of new atoms and/or the rate of mass transport, i.e. diffusion of metal ions to the growing centre. Finally, there is overlap, to be seen as coalescence of the growing clusters, or also, in the case of diffusion control, interference of the diffusion zones.

A modification of the Scharifker and Mostany model was attempted by Sluyters-Rehbach, Wijenberg, Bosco and Sluyters ('SRWBS'). They derived the exact result for independent nuclei in terms of the general nucleation rate law, and demonstrated that in the limit of no overlap the Scharifker and Mostany model is inconsistent with the exact result. In order to avoid this, they considered planar diffusion zones of uniform thickness, with the result that the concentration gradients are uniform over the substrate surface.

Sluyters-Rehbach et al. were the first to consider the general problem of multiple nucleation and growth in the absence of overlap, i.e. they solved the equation for the total current density:

$$j(t) = zFc\pi(2D)^{3/2}\left(\frac{Mc}{\rho}\right)^{1/2}\int_0^t (t-u)^{1/2}\frac{dN}{du}du \qquad (1.28)$$

where $dN/du = AN_0\exp(-Au)$

The solution of above equation is

$$j(t) = zFc\pi(2D)^{3/2}\left(\frac{Mc}{\rho}\right)^{1/2}\frac{N_0}{A^{1/2}}\left\{(At)^{1/2} - e^{-At}\int_0^{(At)^{1/2}} e^{\lambda^2}d\lambda\right\} \qquad (1.29)$$

Also we can write it as

$$j(t) = zFDc\alpha N_0 t^{1/2}\Phi \qquad (1.30)$$

where $\alpha = 2\pi(2MDc/\rho)^{1/2}$ and $\Phi = 1 - \frac{e^{-At}}{(At)^{1/2}}\int_0^{(At)^{1/2}} e^{\lambda^2}d\lambda$

For large values of the argument, $At \geq 20$, $\Phi \rightarrow 1$ and Eq. (1.30) reduces to the case of instantaneous nucleation with the current density proportional to $N_o t^{1/2}$. For small values of At, $At \leq 0.2$, $\Phi \rightarrow (2/3)At$ and the total current density is proportional to $(2/3)N_o At^{3/2}$, the expected result for the limiting case of progressive nucleation. The form of Eq. (1.30) shows that the total current density is equal to the value for the limiting case of instantaneous nucleation multiplied by the function Φ, which reflects the 'retardation' of the current by slow nucleation.

The analysis outlined above becomes invalid when the germinated centers no longer grow independently each other. This is the case if the deposited hemispheres are coalescing, but also earlier when the depletion zones around the start to interfere. The interference has the effect that new nuclei will be formed more at sites on that part of the surface where the concentration of diffusing material is lowered. Moreover, the symmetry of diffusion changes gradually from spherical to planer.

Sluyters-Rehbach et al. has proposed an equation of current density for general case

$$j(t) = zFDc(\pi Dt)^{-1/2}\left(1 - \exp\left[-\alpha N_0(\pi Dt)^{1/2}t^{1/2}\Phi\right]\right) \qquad (1.31)$$

The current transient can be cast in dimensionless form

$$J(At) = \frac{1}{(At)^{1/2}}(1 - \exp[-kAt\Phi]) \qquad (1.32)$$

This equation correctly predicts the value of the current density for both the limits of very short and long times, which makes this model internally consistent.[31, 32, 29]

1.6.4 Heerman and Tarallo Theory

In the model of Sluyters-Rehbach et al. the height of all the diffusion cylinders is the same, independent of the fact of whether the formation of nuclei is either very fast or rather slow. Then, if nucleation is slow, the height of the diffusion cylinder for a nucleus which is born at a later time is grossly overestimated and to compensate for this, the equivalent area of the planar diffusion zone is too large.

The expansion of the diffusion layer should be a function not only of time but also of the nucleation rate constant, i.e. the birth rate of the nuclei. Otherwise, the diffusion layer always expands at the same rate, whether the formation of the nuclei is either very fast or rather slow.

Thus, it is not permitted to use Cottrell's equation with only time variable *t* for the final expression of the current density as is done by Scharifker and Mostany and Sluyters-Rehbach et al. For the real physical situation one can expect that the diffusion layer will become uniform only as the surface of the electrode is covered completely by diffusion zones. However, within the framework of planar diffusion zones, the only reasonable thing to do is to assume that the real diffusion layer in the case of overlap is always uniform.

According to Heerman and Tarallo theory, the current density can be calculated by

$$j(t) = zFDc\frac{1}{(\pi Dt)^{1/2}}\frac{\Phi}{\Theta}\left(1 - \exp\left[-\alpha N_0(\pi Dt)^{1/2}t^{1/2}\Theta\right]\right) \qquad (1.33)$$

Or in dimensionless form

$$J(At) = \frac{1}{(At)^{1/2}}\frac{\Phi}{\Theta}(1 - \exp[-kAt\Theta]) \qquad (1.34)$$

where $\Theta = 1 - (1 - e^{-At})/At$, $\Phi = 1 - \frac{e^{-At}}{(At)^{1/2}}\int_0^{(At)^{1/2}} e^{\lambda^2}d\lambda$ and $\alpha = 2\pi(2MDc/\rho)^{1/2}$

Equation (1.33) reduces to the correct values of current density in the limit of both short and long times. In the case of instantaneous nucleation, $\Phi/\Theta = 1$. In this case the diffusion layer expands as predicted by the Cottrell equation, because all the nuclei are formed at the same time. Eq. (1.33) however, predicts that the current at its maximum will be higher than the Cottrell value and will slowly (dependent on the value of the nucleation rate constant) approach this value after the maximum. This is a logical consequence of the fact that the diffusion layer expands more

slowly, compared with the case of instantaneous nucleation, because the formation of the nuclei occurs at a later time.

For the limiting case of progressive nucleation the current density according to Eq. (1.33) is equal to the value predicted by Scharifker and Mostany multiplied by the constant factor 4/3. Therefore, for both these limiting cases the plots of (I/I_m) vs. t/t_m according to both equations are the same. [32]

1.7 Sonoelectrochemistry

Sonochemistry is the research area in which molecules undergo a chemical reaction due to the application of powerful ultrasound radiation (20 kHz–10 MHz). The physical phenomenon responsible for the sonochemical process is acoustic cavitation [33].

Ultrasound waves, like all sound waves, consist of cycles of compression and expansion. Compression cycles exert a positive pressure on the liquid, pushing the molecules together; expansion cycles exert a negative pressure, pulling the molecules away from one another. During the expansion cycle a sound wave of sufficient intensity can generate cavities. A liquid is held together by attractive forces, which determine the tensile strength of a liquid. In order for a cavity to form, a large negative pressure associated with the expansion cycle of the sound wave is needed to overcome the liquid's tensile strength. The amount of negative pressure needed depends on the type and purity of the liquid. For truly pure liquids, tensile strengths are so great that available ultrasound generators cannot produce enough negative pressure to make cavities. The tensile strength of liquids is reduced by gas trapped in the crevices of small solid particles. When a gas-filled crevice is exposed to a negative-pressure cycle from a sound wave, the reduced pressure makes the gas in the crevice expand until a small bubble is released into solution. Most liquids are sufficiently contaminated by small particles to initiate cavitation.

A bubble in a liquid is inherently unstable. If the bubble is large, it will float away and burst at a surface; if it is small, it will re-dissolve into the liquid. A bubble irradiated with ultrasound, however, continually absorbs energy from alternating compression and expansion cycles of the sound wave. These cause the bubbles to grow and contract, striking a dynamic balance between the vapor inside the bubble and the liquid outside.

Cavity growth depends on the intensity of sound. High-intensity ultrasound can expand the cavity so rapidly during the negative-pressure cycle that the cavity never has a chance to shrink

during the positive-pressure cycle. In this process, therefore, cavities can grow rapidly in the course of a single cycle of sound. For low-intensity ultrasound the size of the cavity oscillates in phase with the expansion and compression cycles. The surface area of a cavity produced by low-intensity ultrasound is slightly greater during expansion cycles than during compression cycles. Since the amount of gas that diffuses in or out of the cavity depends on the surface area, diffusion into the cavity during expansion cycles will be slightly greater than diffusion out during compression cycles. For each cycle of sound, then, the cavity expands a little more than it shrinks. Over many cycles the cavities will grow slowly. The growing cavity can eventually reach a critical size where it will most efficiently absorb energy from the ultrasound. The critical size depends on the frequency of the ultrasound wave. Once a cavity has experienced a very rapid growth caused by either low or high-intensity ultrasound, it can no longer absorb energy as efficiently from the sound waves. Without this energy input the cavity can no longer sustain itself. The liquid rushes in and the cavity implodes. The implosion of cavities establishes an unusual environment for chemical reactions. The gases and vapors inside the cavity are compressed, generating intense heat that raises the temperature of the liquid immediately surrounding the cavity and creates a local hot spot. Even though the temperature of this region is extraordinarily high, the region it itself is so small that the heat dissipates quickly.

The heating and cooling rates during cavitation are more than a billion degrees C per second! This is similar to the cooling that occurs if molten metal is splattered onto a surface cooled near absolute zero. At any given time, therefore, the bulk of the liquid remains at the ambient temperature.

The intensity of cavity implosion, and hence the nature of the reaction, can easily be altered by such factors as acoustic frequency, acoustic intensity, ambient temperature, static pressure, choice of liquid and choice of ambient gas.

Most sonochemical reactions decrease in rate with increasing ambient temperature, i.e., the temperature outside the cavity. The higher the ambient temperature is, the more vapor there will be inside the cavity. The extra vapor cushions the implosion of the cavity and lowers the temperature of implosion. Therefore sonochemical reactions proceed more slowly as ambient temperature increases. Sonochemical reactions do not depend greatly on frequency. The major effect of frequency is to change the critical size of a cavity before implosion, which does not change the cavitation process significantly.

The dynamics of cavity growth and implosion are strongly dependent on local conditions, including the form of the materials: whether they are liquids, extended solid surfaces in liquids or solid particles in liquids. The sonochemistry of liquids depends mainly on physical effects of the quick heating and cooling caused by cavity implosion. The sonochemistry of solid surfaces in liquids depends on a change in the dynamics of cavity implosion. The presence of the surface distorts the pressure from the ultrasound field so that a cavity implosion near a surface is markedly asymmetric. This generates a jet of liquid directed at the surface that moves at speeds of roughly 400 kilometers per hour. The jet, as well as the shock waves from cavity implosion, erode solid surfaces, remove nonreactive coatings and fragment brittle powders. Reactions are further facilitated by high temperatures and pressures associated with cavity implosion near surfaces [34].

Ultrasound keeps the electrode surface clean and improves mass transport such that uniform electrode reaction occurs across the area of a centimeter-scale electrode, with consequently greater reaction velocity at the electrodes [35]. Ultrasound was also shown to affect metal electrodeposition with benefit to the quality of the deposit, its adhesion and morphology, and also the diminution of brighteners and other additives needed in silent systems. The effects of ultrasound in a liquid are to cause ‘acoustic streaming’ and/or the formation of cavitation bubbles, depending upon the parameters of ultrasonic power, frequency, sonic source characteristics, and solution phenomena such as viscosity, volatility, and the presence of dissolved gases or other nucleation sites [36].

A number of possible effects of ultrasound upon an electrochemical system may be predicted:

- A general improvement of hydrodynamics and movement of species;
- The alteration of concentration gradients at various points in the reaction profile, and consequent switching of kinetic regimes with effect on mechanism and reaction products;
- A cleaning and abrading effect upon an electrode surface, thus obviating fouling problems, or else altering the nature of coatings that manage to form;
- Sonochemically-induced reactions of intermediate species that have been generated electrochemically;
- The sonochemical formation of species that react electrochemically in conditions where the silent system is electroinactive [36].

The deposition of metals under the influence of ultrasound has received significant attention as sonication is thought to confer various benefits over conventional silent electrodeposition or plating. These are claimed to include increased deposit hardness, enlarged film thickness, improved deposition rates and efficiencies, and greater adhesion of the deposit to the electrode. These effects are attributed to factors such as: acoustic streaming increasing transport of active species to the electrode surface, continuous cleaning/activation of the electrode (particularly in passivating media), effects resulting from the appearance and collapse of cavitational bubbles, and ultrasonic degassing of solutions. In electrodeposition/plating under the influence of ultrasound, the critical effect is the increase in mass transport, which may be high enough to change a diffusion controlled system into a charge controlled system. Ultrasound also ablates material from the electrode surface, but has no effect on growth via charge transfer from the electrode to the metal ion [37].

1.8 Objectives

- Synthesis of ultra fine/nano copper thin films through sonoelectrochemical route at various operating parameters.

- Characterization of the above deposits by X-RD, SEM, EDX, AFM.

- Study of properties like hardness of fabricated films by nanoindentation.

Chapter 2

Experimental section

Experimental Section

2.1 Experimental Setup

Electrochemical studies or experiments were conducted with a potentiostat/galvenostate (Eco Chemie Netherland, Autolab PGSTAT 12) system having computer interface of GPES software and three electrode electrochemical cell. Experiments were performed on O_2 free brass substrates of exposed surface area of 1.5 cm × 1.5 cm. A platinum rod of 0.2 cm diameter and an Ag/AgCl electrode (Eco Chemie, Netherlands) served as counter and reference electrodes respectively. Before each scan and subsequent experiment, electrodes were polished, washed and dried properly. Ultrasound irradiation was accomplished by a 20 kHz ultrasonic horn with 20% output power transducer system (Sonics & Materials, VCF1500) fitted with a titanium tip. Low temperature electrodeposition and low temperature sonoelectrodeposition studies were done with the electrochemical cell placed in refrigerator which temperature varies from room temperature to −20 °C. The temperature of electrolyte solution was measured with digital thermometer.

2.2 Substrate preparation

Prior to the film deposition brass substrates were polished with emery papers followed by a diamond paste polishing on a polishing cloth in order to remove met nature of the surface and to get mirror like finish. The reproducibility of the results obtained depends on the quality of the polishing. After polishing, the substrates were cleaned with acetone and rinsed in distilled water. The dart particles on the surface of the substrate can adversely affect the nucleation and growth processes during film growth and can also lead to the inclusions or formation of many impurities. Hence it was important to clean substrates properly before they were put into the film deposition system.

2.3 Electrolytic Bath preparation

The plating bath contains $CuSO_4.5H_2O$ and 98% conc. H_2SO_4. Conc. H_2SO_4 is used for making solution conductive. All chemicals were from commercial sources and were the highest purity available. They were used without further purification. Solution was prepared from an

additive free copper sulphate bath in doubly distilled water at room temperature and under moderate agitation. All solutions in this study were prepared from doubly distilled water.

2.4 Synthesis

Electrodeposition is used as a route to fabricate copper thin film. The deposition was commenced in potentiostatic mode. The operating parameters are variation in bath temperature, varying copper ion concentration and varying pH with sulphuric acid. The different bath temperature used were 25 °C, 5 °C, − 0.5 °C, − 2.5 °C, and − 4 °C with 0.1 M $CuSO_4.5H_2O$ and 60 gpl H_2SO_4 concentration. Copper concentration variation ranges from 0.025M, 0.05M, and 0.1M with 60 gpl acid concentration. These experiments conducted at room temperature. Acid concentration has been changed from 20 gpl to 50 gpl with an interval of 10 gpl. The deposition time and deposition potential of all above experiments were 30 sec and −0.45V respectively. All experiments have been conducted in silent and sonication condition.

2.5 Electrochemical analysis

The electrochemical phase formation are studied by various methods including cyclic voltammetry (CV), double pulse techniques, linear sweep voltammetry (LSV), impedance spectroscopy, chronoamperometry (CA)/chronopotentiometry (CP), voltammetry analysis (differential pulse, square wave, sampled DC, AC 2^{nd} harmonic, differential normal pulse), potentiometric stripping analysis etc. Here the basic principles underlying CV and CA are described, as they have been used in the analysis and synthesis of the copper thin films.

2.5.1 Cyclic Voltammetry (CV)

Cyclic voltammetry is characterized by smooth increase of a working electrode potential from one potential limit to the other and back. It follows that the potential limits and the potential sweep rate are the basic adjustable parameters. Also the properties of an electrolyte, mainly the concentration of electroactive species and temperature, could be affected. In this technique, the input potential signal is a potential of a stationary working electrode is scanned linearly by means of potentiostat and the resulting current is monitored. When the current is plotted versus the potential, a cyclic voltammogram curve is obtained. There are two different regions can be

recognized in the resulting cyclic voltammogram; anodic (positive current values) and cathodic (negative current values) where the oxidation and reduction reactions take place, respectively. The peak current on this voltammogram shows the potential where the electrode reactions take place. The potential, shape, and the height of the peak current are functions of scan rate, electrode materials, and solution composition. Generally, two limiting cases of studied systems do exist. It is a reversible electrode process and an irreversible electrode process.

The reversibility of an electrochemical reaction will depend on the rate of electron transfer at the electrode. If the rate of electron transfer is fast with respect to the timescale of the CV experiment, then the reaction is reversible, and the peak current (i_p) at 25 °C can be expressed by the Randles-Sevcik equation

$$i_p = (2.69 \times 10^5) n^{3/2} A C D^{1/2} \nu^{1/2} \qquad (2.1)$$

where n is the number of moles of electrons transferred in the reaction, A is the area of the electrode, C is the analyte concentration (in moles/cm^3), D is the diffusion coefficient, and ν is the scan rate of the applied potential.

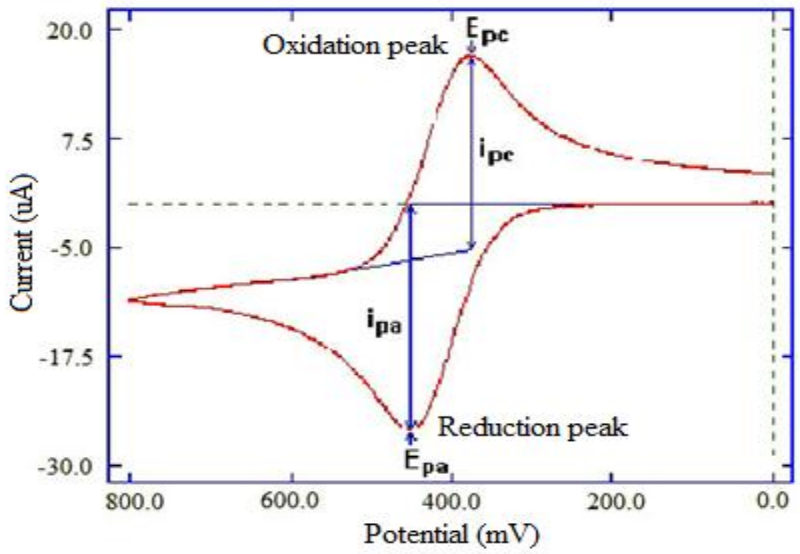

Figure 2.1: A typical cyclic voltammogram showing reduction and oxidation current peaks

For an irreversible electrochemical reaction, the rate of electron transfer is slow with respect to the timescale of the experiment, such that the rate of diffusion is greater than the rate of electron

transfer. A totally irreversible system will have no reverse peak. In this case, the peak current is given by:

$$i_p = (2.99 \times 10^5) n(\alpha n_a)^{1/2} A C D^{1/2} \nu^{1/2} \quad (2.2)$$

where α is the transfer coefficient. The peak current is lower in height than reversible systems and depends on the value of α. [38, 39]

2.5.2 Chronoamperometry (CA)

Chronoamperometry (CA) is an electrochemical method in which a step potential is applied and the current, i (A), is measured as a function of time, t (s). This i-t response is comprised of two components: the current due to charging the double-layer and the other due to the electron transfer reaction with the electroactive species. When the working electrode is immersed in the electrolytic solution, a very thin region called the double layer is formed at the electrode-electrolyte interface. The double layer contains a distribution of ions at the interface and is considered to work as a capacitor (C) that represents the electrode double-layer capacitance. It is instructive to model this situation as being analogous to charging a capacitor at the initial potential step.

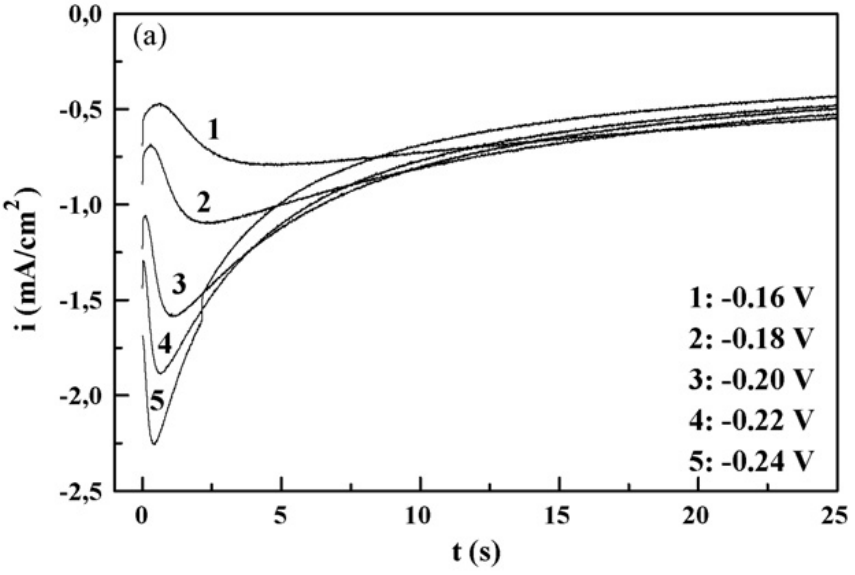

Figure 2.2: Current transients for Cu deposition on FTO substrates at different applied potentials.

The i-E wave obtained with cyclic voltammetry is used to calculate C. That is, the charge, q, is given by: q = it = CAE where E is the potential of the electrode (vs. reference electrode). The extent to which both occur simultaneously depends on the initial and the final value of the potential. The results are most easily interpreted when a planar (flat) electrode is used in a quiet, unstirred solution, and the applied potential is sufficient to reduce or oxidize the electroactive species as fast as it gets to the electrode surface, i.e., at a diffusion-controlled rate.

The current (i.e., electrons) flows to the working electrode (WE) in order to bring its potential to some desired value. A potentiostat with a 3-electrode cell provides the current via the auxiliary electrode (AE) to the WE while the potential is measured with respect to a reference electrode (RE).

Let us examine now a current, i, vs. time t, response in the presence of an electroactive species that undergoes an electron transfer reaction at a diffusion-controlled rate. Under these conditions, the current decay is given by

$$i = \frac{nFAD^{1/2}C^{b}}{(\pi t)^{1/2}} \qquad (2.3)$$

where n is the number of electron(s) transferred per electroactive molecule or ion; F is Faraday's constant; A is the area of the electrode surface in cm^2; D is the diffusion coefficient in cm^2/s; C^b is the concentration of the electroactive species in mol/cm^3; and t is time in second. The current raises rapidly to a maximum value decays as a function of $t^{1/2}$, as seen in figure (2.2). [40, 27]

2.6 Characterization techniques

Several techniques have been used to characterize the electrodeposits and sonoelectrodeposits of copper thin film. The X-ray diffraction, in the range of scanning angel 30-150° at a scanning rate 2° with CuKα radiation (λ=1.5406A^0) using Philips X' PERT System X-Ray Diffractometer. JEOL scanning electron microscope (SEM) at low acceleration voltages, and atomic force microscope (AFM) were employed to examine the morphology, particle size and microstructure of the electrodeposits and sonoelectrodeposits of thin film at the various temperatures. The chemical composition/purity of the electrodeposits and sonoelectrodeposits was determined by energy dispersive spectroscopy (EDS) analysis. Mechanical properties were

studied by nanoindentation. And Schrifkar and Hills model of nucleation and growth are used to study the nucleation and growth mechanism.

2.6.1 X-Ray Diffraction

X-ray scattering techniques are a family of non-destructive analytical techniques which reveal information about the crystallographic structure, chemical composition, and physical properties of materials and thin films.

2.6.1.1 Diffraction and Bragg's Equation

The interaction of waves with periodic structures produces diffraction effects if the wavelength and the periodicity of the crystals, are of similar magnitude. X-rays may easily be produced with wavelengths matching the unit cell dimensions of crystals, but electrons or neutrons of appropriate energy can also be used for diffraction experiments on crystals.

Electromagnetic waves with wavelengths of the order of 10^{-10} m are called X-rays. The electric field of such waves interacts with the charges of all electrons of an atom, which then emit an almost spherical wave with the same wavelength as the incident radiation. The amplitude of this outgoing wave is proportional to the number of electrons in the atom, and, hence, to the atomic number. Light elements with few electrons, e.g., carbon or oxygen, are therefore "poor" scatterers for X-rays, whereas heavy elements such as lead are "good" scatterers. Detection limits are severely influenced by this effect.

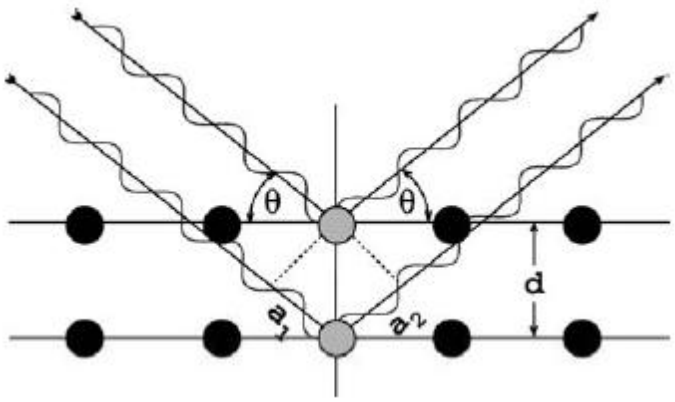

Fig2.3: Geometric derivation of Bragg's law

Without any diffraction effects, the incidence of a primary X-ray beam onto a sample volume would produce scattering in all directions. Diffraction redistributes intensity from the whole

scattering sphere into distinct directions. Therefore, intensity peaks arise in certain directions, whereas in directions between peaks the intensity decreases drastically. The intensity integrated over the sphere, however, remains constant due to energy conservation. Constructive interference and hence a so called Bragg reflection is obtained when the path of the wavelet scattered of the lower of the two planes is longer by an integer number of wavelengths λ than that of the wavelet scattered off the upper plane. A reflection will thus occur when

$$n\lambda = 2d\ sin\theta \qquad (2.4)$$

This is the so-called Bragg equation, where λ is the wavelength of the radiation, n is an integer number, θ is the angle between the lattice planes and the incident beam and d is the distance of the lattice planes for which the peak occurs [41].

The mechanical assembly that makes up the sample holder, detector arm and associated gearing is referred to as goniometer [42].

X-ray diffraction peaks are broadened due to instrumental effects, small particle size, and lattice strain in the material [43]. The crystallite size is determined by measuring the Bragg peak width at half the maximum intensity and putting its value in scherrer's formula. The crystallite size and lattice strain in the powder particles can be determined by the X-ray peak broadening techniques. Average crystallite sizes of copper deposit were determined by the Williamson-Hall formula (As Scherrer equation is valid only for powders or loosely bound deposits but not for hard and adherent deposits).

The contribution of the particle size and non-uniform strain in the grains to the observed X-ray line broadening, β, are considered to be additive generating the formula as:

$$\beta_{total} = \beta_{particle\ \ size} + \beta_{strain} \qquad (2.5)$$

The contribution of broadening due to small particle size is given by Scherrer equation while the broadening due to strain is represented by differentiation of Bragg's law. The total broadening (β_{total}) is the measured FWHM in radians, corrected for instrumental broadening. The X-ray wavelength of the source Cu K_α is λ = 0.15418 nm, where t is the particle size, and 4 ($\Delta d/d$) represents the strain. Multiplying both sides of the equation by cos θ gives the final form,

$$\beta_{total}\ \cos\theta = \frac{0.94\lambda}{t} + \ 4\sin\theta\left(\frac{\Delta d}{d}\right) \qquad (2.6)$$

which is used to calculate the particle size and lattice strain of the copper deposit from the plot of $\beta_{total}\cos\theta$ versus $\sin\theta$ [21].

2.6.2 Scanning Electron Microscopy

In SEM, a source of electrons is focused in vacuum into a fine probe that is rastered over the surface of the specimen. The electron beam passes through scan coils and objective lens that deflect horizontally and vertically so that the beam scans the surface of the sample. As the electrons penetrate the surface, a number of interactions occur that can result in the emission of electrons or photons from or through the surface. A reasonable fraction of the electrons emitted can be collected by appropriate detectors, and the output can be used to modulate the brightness of a cathode ray tube (CRT) whose x- and y- inputs are driven in synchronism with the x-y voltages rastering the electron beam. In this way an image is produced on the CRT; every point that the beam strikes on the sample is mapped directly onto a corresponding point on the screen. SEM works on a voltage between 2 to 50 kV and its beam diameter that scans the specimen is 5nm-2μm. The principle images produced in SEM are of three types:

- **Secondary electron images**, Secondary electrons are produced when an incident electron excites an electron in the sample and loses most of its energy in the process. The excited electron moves towards the surface of the sample undergoing elastic and inelastic collisions until it reaches the surface, where it can escape if it still has sufficient energy. Production of secondary electrons is very topography related. Due to their low energy (5eV) only secondaries that are very near the surface (<10 nm) can exit the sample and be examined. Any changes in topography in the sample that are larger than this sampling depth will change the yield of secondaries due to collection efficiencies. Collection of these electrons is aided by using a "collector" in conjunction with the secondary electron detector.
- **Backscattered electron images,** Backscattered electrons consist of high-energy electrons originating in the electron beam, that are reflected or back-scattered out of the specimen

interaction volume. The production of backscattered electrons varies directly with the specimen's atomic number. This differing production rates causes higher atomic number elements to appear brighter than lower atomic number elements. Backscattered are used to form diffraction images, called EBDS, that describe the crystallographic structure of the sample.

- **Elemental X-ray maps,** inelastic scattering, place the atom in an excited (unstable) state. The atom "wants" to return to a ground or unexcited state. Therefore, at a later time the atoms will relax giving off the excess energy. X-Rays, cathodoluminescence and Auger electrons are three ways of relaxation. X-rays are collected to contribute in Energy Dispersive X-ray Analysis (EDX or EDS), which is used to the topography of the chemical composition of the sample.

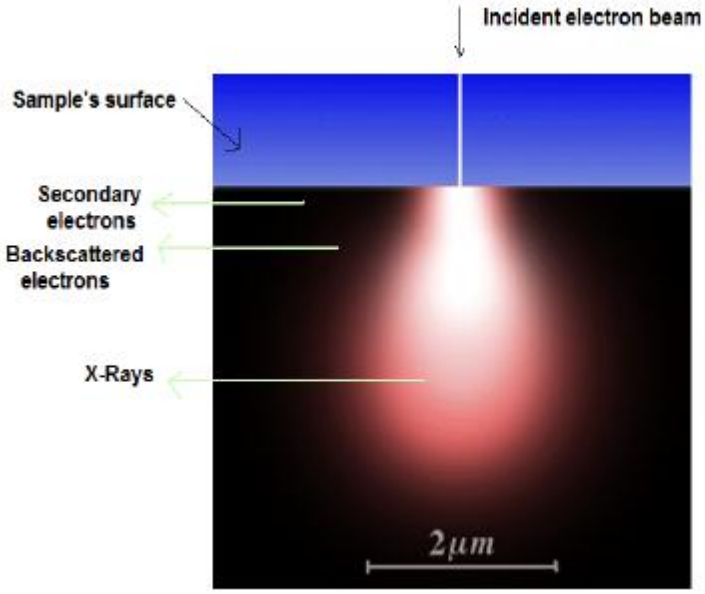

Figure 2.4: Generalized illustration of interaction volumes for various electron-specimen interactions

Secondary and backscattered electrons are conventionally separated according to their energies. When the energy of the emitted electron is less than about 50eV, it is referred as a secondary electron and backscattered electrons are considered to be the electrons that exit the specimen with energy greater than 50eV. Detectors of each type of electrons are placed in the microscope in proper positions to collect them. Disadvantages of SEM are, SEM is only used for surface images and both resolution and crystallographic information is limited, samples must be conductive, so non-conductive materials are carbon coated [44].

2.6.3 Energy dispersive X-ray analysis

EDX Analysis stands for Energy Dispersive X-ray analysis. It is sometimes referred to also as EDS or EDAX analysis. It is a technique used for identifying the elemental composition of the specimen, or an area of interest thereof.

The EDX analysis system works as an integrated feature of a scanning electron microscope (SEM), and cannot operate on its own without the latter. During EDX Analysis, the specimen is bombarded with an electron beam inside the scanning electron microscope. The bombarding electrons collide with the specimen atoms' own electrons, knocking some of them off in the process. A position vacated by an ejected inner shell electron is eventually occupied by a higher-energy electron from an outer shell. To be able to do so, however, the transferring outer electron must give up some of its energy by emitting an X-ray. The amount of energy released by the transferring electron depends on which shell it is transferring from, as well as which shell it is transferring to. Furthermore, the atom of every element releases X-rays with unique amounts of energy during the transferring process. Thus, by measuring the amounts of energy present in the X-rays being released by a specimen during electron beam bombardment, the identity of the atom from which the X-ray was emitted can be established.

The output of an EDX analysis is an EDX spectrum. The EDX spectrum is just a plot of how frequently an X-ray is received for each energy level. An EDX spectrum normally displays peaks corresponding to the energy levels for which the most X-rays had been received. Each of these peaks is unique to an atom, and therefore corresponds to a single element. The higher a peak in a spectrum, the more concentrated the element is in the specimen [45].

An EDX spectrum plot not only identifies the element corresponding to each of its peaks, but the type of X-ray to which it corresponds as well. For example, a peak corresponding to the amount of energy possessed by X-rays emitted by an electron in the L-shell going down to the K-shell is identified as a K-Alpha peak. The peak corresponding to X-rays emitted by M-shell electrons going to the K-shell is identified as a K-Beta peak.

2.6.4 Atomic Force Microscopy

The Atomic Force Microscope is an instrument that can analyze and characterize samples at the microscope level. This means we can look at surface characteristics with very accurate resolution ranging from 100 μm to less than 1μm.

Whatever the origin of the force, all force microscopes have five essential components:

1. A sharp tip mounted on a soft cantilever spring
2. A way of sensing the cantilever's deflection
3. A feedback system to monitor and control of deflection (and, hence, the interaction force)
4. A mechanical scanning system (usually piezoelectric) that moves the sample with respect to the tip in a raster pattern
5. A display system that converts the measured data into an image [46]

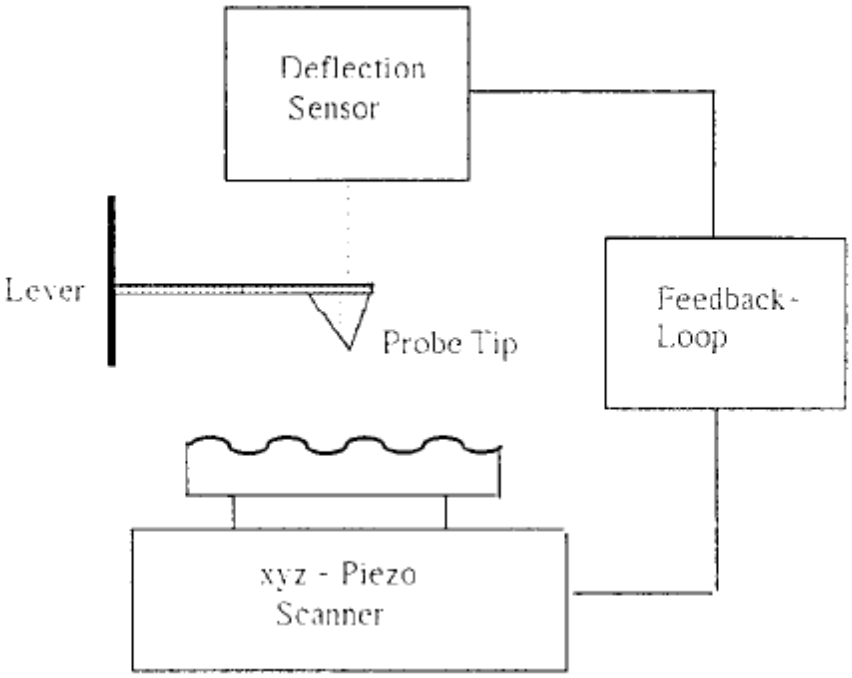

Figure 2.5: Basic principle of AFM

In force microscopy the probing tip is attached to a cantilever type spring. In response to the force between tip and sample the cantilever, also called lever, is deflected. Images are taken by scanning the sample relative to the probing tip and digitizing the deflection of the lever or the z-movement of the piezo as a function of the lateral position x, y. Typical spring constants are between 0.001 to 100N/m and motions from microns to ≈0.1Å are measured by the deflection sensor. Typical forces between probing tip and sample range from 10^{-11} to 10^{-9}N at separations of ≈Å. Therefore, non destructive imagining is possible with these small forces. Two force regims are distinguished: contact and non contact mode. When the microscope is operated in non contact mode at tip-sample separations of 10 to 100nm, forces, such as Vander Waals,

electrostatic, magnetic or capillary forces, can be sensed and give information about surface topography, distribution of charges, magnetic domain wall structure or liquid film distribution. At smaller seperations of the order of Å the probing tip is in contact with the sample. In this mode, ionic repulsion forces allow the surface topography to be traces with high resolution. Under best condition atomic resolution is achieved [47]. To achieve atomic resolution with AFM, a first necessary condition is that the mechanical vibrations between tip and sample are smaller than the atomic corrugations [48]. In addition, frictional forces and elastic and plastic deformations can be detected under appropriate conditions [47].

2.6.5 Nanoindentation

Indentation has been the most commonly used technique to measure the mechanical properties of materials because of the ease and speed with which it can be carried out. Indentation load–displacement data contain a wealth of information. From the load – displacement data, many mechanical properties such as hardness and elastic modulus can be determined without imaging the indentations.

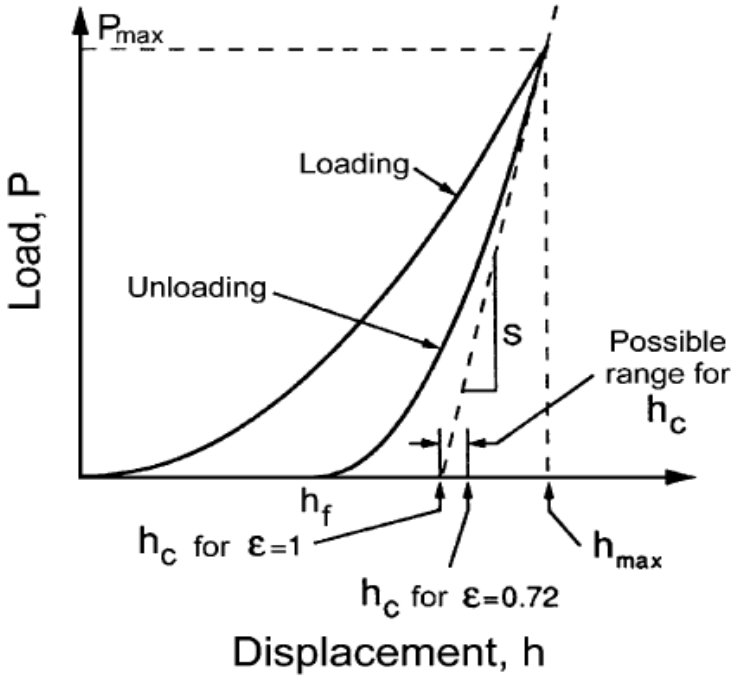

Figure 2.6: Typical load-displacement curve

The nano-indenter has been used to estimate the fracture toughness of ultrathin films, which cannot be measured by conventional indentation tests. Diamond is the most frequently used

indenter material, because its high hardness and elastic modulus minimize the contribution of the indenter itself to the measured displacement. For probing properties such as hardness and elastic modulus at the smallest possible scales, the Berkovich triangular pyramidal indenter is preferred over the four-sided Vickers or Knoop indenter because a three-sided pyramid is more easily ground to a sharp point.

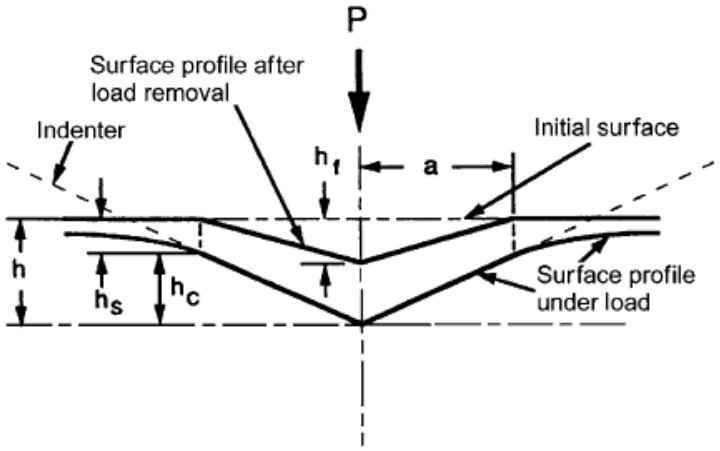

Figure 2.7: the deformation pattern of an elastic-plastic sample during and after indentation.

The two mechanical properties measured most frequently using indentation techniques are the hardness, H, and the elastic modulus, E. As the indenter is pressed into the sample, both elastic and plastic deformation occurs, which results in the formation of a hardness impression conforming to the shape of the indenter. During indenter withdrawal, only the elastic portion of the displacement is recovered, which facilitates the use of an elastic solution in modeling the contact process.

In Fig. 2.6, h_{max} represents the displacement at the peak load, P_{max}. h_c is the contact depth and is defined as the depth of the indenter in contact with the sample under load. h_f is the final displacement after complete unloading. S is the initial unloading contact stiffness.
Nanoindentation hardness is defined as the indentation load divided by the projected contact area of the indentation. It is the mean pressure that a material can support under load. From the load–displacement curve, hardness, H, can be obtained at the peak load as

$$H = \frac{P_{max}}{A} \qquad (2.7)$$

where A is the projected contact area. Measurement of the projected contact area from a load displacement curve requires the contact depth, h_c,

$$h_c = h_{max} - \varepsilon \frac{P_{max}}{S} \tag{2.8}$$

where ε is a constant that depend on indenter geometry (ε = 0.75 for a Berkovich indenter).
The elastic modulus of the indented sample can be inferred from the initial unloading contact stiffness $S = {dP}/{dh}$, i.e., the slope of the initial portion of the unloading curve.
A geometry-independent relation involving contact stiffness, contact area, and elastic modulus can be derived as follows

$$S = 2\beta \sqrt{\frac{A}{\pi}} E_r \tag{2.9}$$

Where β is a constant that depends on the geometry of the indenter (β=1.034 for a Berkovich indenter) and E_r is the reduced elastic modulus, which accounts for the fact that elastic deformation occurs in both the sample and the indenter. E_r is given by

$$E_r = \frac{1 - \nu^2}{E} + \frac{1 - \nu_i^2}{E_i} \tag{2.10}$$

where E and ν are the elastic modulus and Poisson's ratio for the sample, respectively, and E_i and ν_i are the same quantities for the indenter. For diamond, E_i = 1141 GPa and ν_i = 0.07. [49]

Chapter 3

Results and Discussion

Results and Discussions

3.1 Cyclic Voltammetry (CV)

Cyclic voltammetry (CV) was performed in the [0.8 to –0.6] V potential range to identify the presence of the electrodeposition processes and to verify the electrochemical behavior of the electrodes in the elctrodeposition bath. Figure 3.1 shows typical CVs for brass electrodes obtained with a scan rate of 10 mV/s. Both voltammograms are characterized by the presence of cathodic-anodic peaks associated with deposition and dissolution of Cu. Furthermore, in the two curves, it is possible to note the presence of crossovers of the cathodic and anodic branches, typical of the formation of a new phase, involving a nucleation followed by diffusion limited growth process.

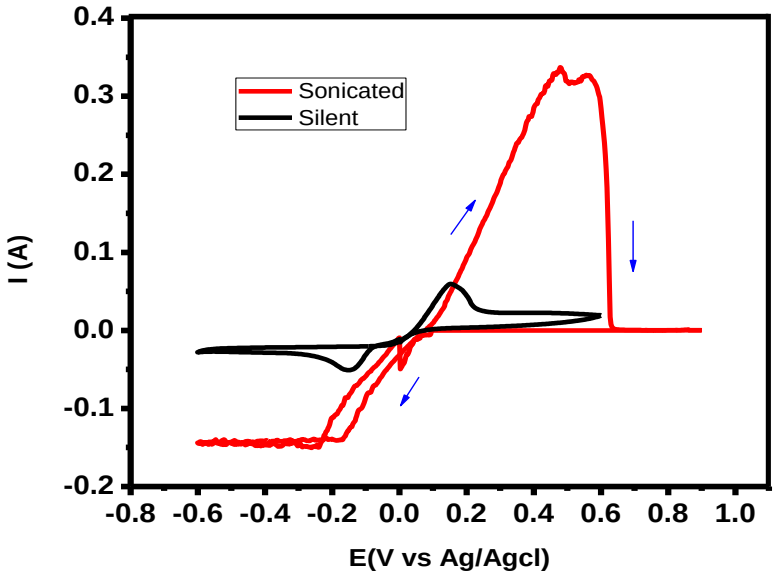

Figure 3.1 Cyclic voltammetry of copper deposition on brass under silent and sonication at a scan rate of 10 mV/s

Notable beginning of current decrease was detected at –0.001 V vs. Ag/AgCl. It is clear from the voltammogram under silent conditions that a sharp rising cathodic current is observed as the potential is swept to –0.083 V. Under ultrasonic irradiation this sharp peak is also observed at

−0.261 V, however, the current magnitude is almost three times greater than that under silent condition. This observation is consistent with the fact that ultrasound increases mass transport to and from electrode surface. On reversing the scan direction, metal already deposited on the electrode surface continues to grow as a result of the $Cu^{2+}(aq) + 2e^{-} = Cu(s)$ reaction remaining thermodynamically and kinetically favorable. Sharp almost symmetric anodic peaks are observed under both silent and insonated conditions when the potential is swept in positive direction. These are located 0.183 and 0.479 V for silent and insonated conditions, respectively, and both correspond to the dissolution of the deposited copper layer. The key features of the CVs are presented in Table 3.1. It is apparent from the table that there is a significant increase in the amount of Cu deposited under sonic agitation favoring the hypothesis of increased mass transport.

Table 3.1: Key features of CV for Cu deposition under silent and insonated conditions

Item	Silent	Sonication
Cathode depositing peak potential/V	–0.083	–0.261
Anodic stripping peak potential/V	0.183	0.479
Cathode depositing peak height/A	−0.050	–0.150
Anodic stripping peak height/A	0.065	0.337
Cathode depositing peak area/C	–3.056	−14.75
Anodic stripping peak area/C	2.174	11.14

However the cleaning in insonated condition is quite effective as there is a sharp drop in anodic current to a zero value in comparison to a nearly zero value of current for silent deposition. These observations support the fact of in-situ cleaning of the electrodes by ultrasound. Fig. 3.1 also indicates copper can be deposited at a potential positive than the reverse potential and that underpotential Cu deposition does occur under insonation. The presence of underpotential

deposition indicates a strong deposit-substrate interaction, i.e. the early stages of the electrodeposition of Cu correspond to a Volmer-Weber growth mechanism [2]**.** Hence sonication should produce an adherent deposit as compared to silent one. As deposition occurs throughout the negative potential regime, we choose a potential of –0.45 V for experimentation in all the operating conditions.

3.2 Sonication Impact

As discussed in section 1.7, sonication capable of creating zones of extremely high level of localized supersaturation should set off the nucleation process. The above effect on crystallization process has been reported for a number of systems [50, 21]. Crystal fragmentation by ultrasound may create new steps on the defect free crystal face to further supplement the crystallization process. The ultrasonic energy is believed to stimulate a biphasic nucleation sequence i.e. primary (on the native substrate) and secondary (on the existing primary clusters). Hence insonation of liquids will promote the nucleation process to a greater extent than the silent condition alone. Before experimenting the coupling effect, an attempt has been made to establish the effect of ultrasound.

Researchers have employed fast linear sweep voltammetry (LSV) and cyclic voltammetry (CV) [51, 52] to observe the quantitative mass transport transient events. The methods introduce potential driven supersaturation and hence there may not be an effortless clear prediction of the effects. However, little attention has been paid to sonoelectrochemically modified time dependent current analysis. An attempt has been made here to experiment the above effects through sono-chronoamperometric current transient (SCCT).

The CCTs are shown in Fig. 3.2. The results disagree with the reports for cobalt deposition on glassy carbon electrode [53]. All the SCCTs have a sharp initial decrease in current followed by irregular troughs and crests like current responses. The early fall is due to double layer charging at the electrode surface. The rest current progression may not be inferred as noise (2 s persistence). If it would have been the sole impact of truncation in diffusion spheres then the rising current should have still higher values. Thus we did interpret these irregularities as a sequence of nucleation loops. The SCCTs have the initial loop at around 3 s and the successive

loops have abounded with same time occurrence. It was understood that the preliminary loops may be due to the conventional 3D nucleation and growth.

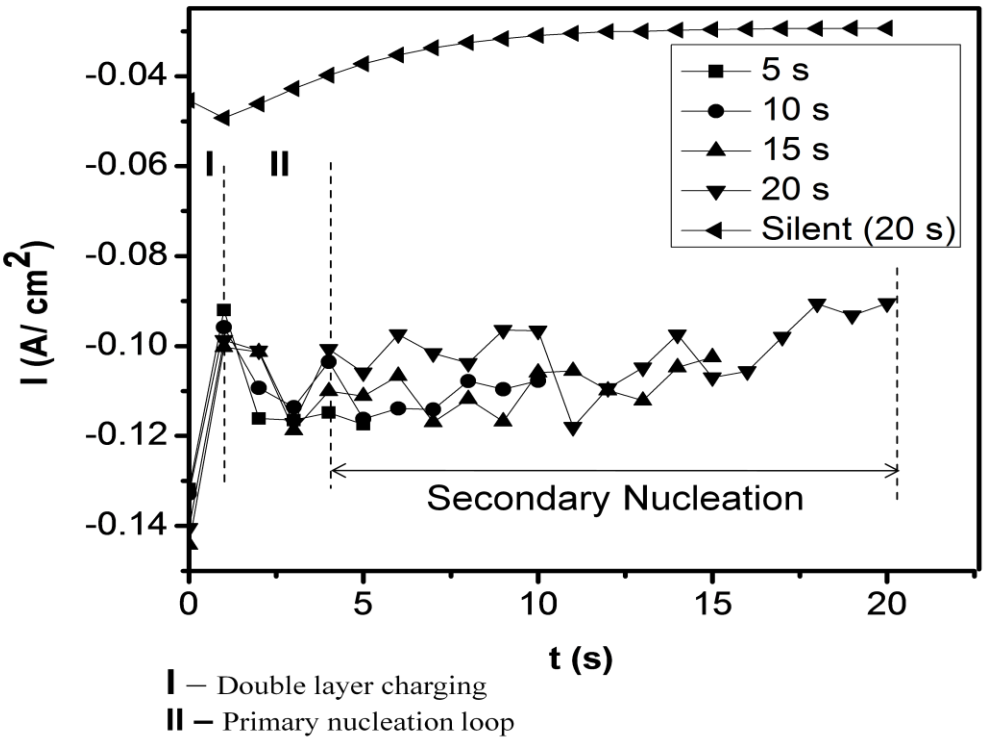

Figure 3.2: Chronoamperometric current transients for Cu deposits under insonation for different time periods

The progressive loops should support the hypothesis of secondary nucleation by crystal breakage [21, 50]. The experiment has also been extended without ultrasonic transient environment for evolving the differential crystal breakage. The silent CCT defers from the SCCT following a typical transient of rising portion and then a decaying current obeying the Cottrell law. The kinetics parameters were calculated using the Scharfiker's general equation for instantaneous nucleation [26].

The slope of log(current density) vs log(time) varied from 0.4-0.55, indicates instantaneous phase appearance (not shown). Table 3.2 shows characteristic kinetics parameters along with total charge involved in the deposition process. The total charge consumed varies from 0.764 –

2.05 C. A total charge of 0.713 C has been consumed for silent deposit at 20 s in compared to a value of 2.05 C with sonication.

Table 3.2: Characteristic Kinetics Parameters of *i(t)* transients obtained for sonicated Cu deposits for different deposition time periods

Time (Sec)	I_{max}(A/cm^2)	t_{max} (S)	D × 10^{-4} (cm^2 s^{-1})	$N_{0\ (P)}$ × 10^3 (cm^{-2})	$N_{0\ (S)}$ × 10^3 (cm^{-2})	$N_{0\ (T)}$ × 10^3 (cm^{-2})	Q_{total}(exp) C
5	0.116	3	6.6	1.52	–	1.52	0.764
10	0.114	3	6.4	1.56	3	4.56	1.1
15	0.118	3	6.8	1.48	4.2	5.68	1.69
20	0.117	3	6.7	1.5	6.1	7.7	2.05(0.713silent)

Electrolyte media: 6.35 g l^{-1} $CuSO_4$. $5H_2O$ + 60 g l^{-1} H_2SO_4, Deposition potential: – 0.45V

The difference may be attributed to the nucleation phenomena, as explained later. The table also contains the nuclei number density calculated for secondary nucleation, $N_{0\ (S)}$ following the same model. The diffusion coefficient calculated in silent condition was 1.1 × 10^{-5} (cm^2 s^{-1}) compared with the values of 0.8-1.5× 10^{-5} (cm^2 s^{-1}) published elsewhere, while in the presence of ultrasound, the diffusion coefficient has increased to values, 6.4-6.8 × 10^{-4} (cm^2 s^{-1}). The calculated nuclei number density for primary nucleation, $N_{0\ (P)}$, for all the time period is approximately same. The number density for the secondary nucleation is increasing with increasing time period i.e. 3-6.1 × 10^3 (cm^{-2}). However the rate of increase of number of secondary nuclei decreases with time. This may be explained by the fact that, due to degassing at the electrodes, deposits are highly adherent under insonation [21]. Thus the process of crystal breakage may not possible further for protracted sonication.

AFM micrographs are shown in Fig 3.3 for 5 s, 10 s, 15 s and 20 s. It can be noticed that at 5 s the grains fall within the range of 210 – 260 nm height with a roughness factor of 47 nm. As the time of deposition increases the standard deviation of the grain distribution becomes narrow and smooth. The deposit at 20 s is the finest. Most of the grains fall in the height range of 10 – 30

nm. A total analysis of the area and volumetric analysis is given in Table 3.3. This result can be interpreted as in the following ways.

Table 3.3: Roughness factor and grain size distributions from AFM measurements

Time	Grain distribution (nm - nm)	Roughness factor (nm)	Average height (nm)	Thickness (nm)	
				Calculated*	Measured
5	210-260	47	201	280	266
10	90-134	23	100	405	418
15	50-80	19	60	624	612
20	10-30	15	42	757	759

Ultrasound is capable of crystal breakage produces smaller grains and balances the heights of grains. This in result smoothens the surfaces at longer period of deposition. The peak and valley method of AFM analysis has been used to measure the thickness of the films. Fig. 3.4 shows the above method for the deposition at 20 s.

The micrograph along with the line analysis also shows a nearly smooth and uniform deposit. The measured and calculated values of thickness are given in Table 3.3. Calculations of thickness of the films are done according to the formula given in equation 3.1.

$$Thickness\ (cm) = \frac{QM}{zFA\rho} \qquad (3.1)$$

Where, Q = Charge (C), M = Molecular weight of copper (63.55), F= Faraday Constant (96500 $C.mol^{-1}$), A = Area (cm^2), ρ= density of copper (8.89 $g.cm^{-3}$), z = No. of electrons transferred.

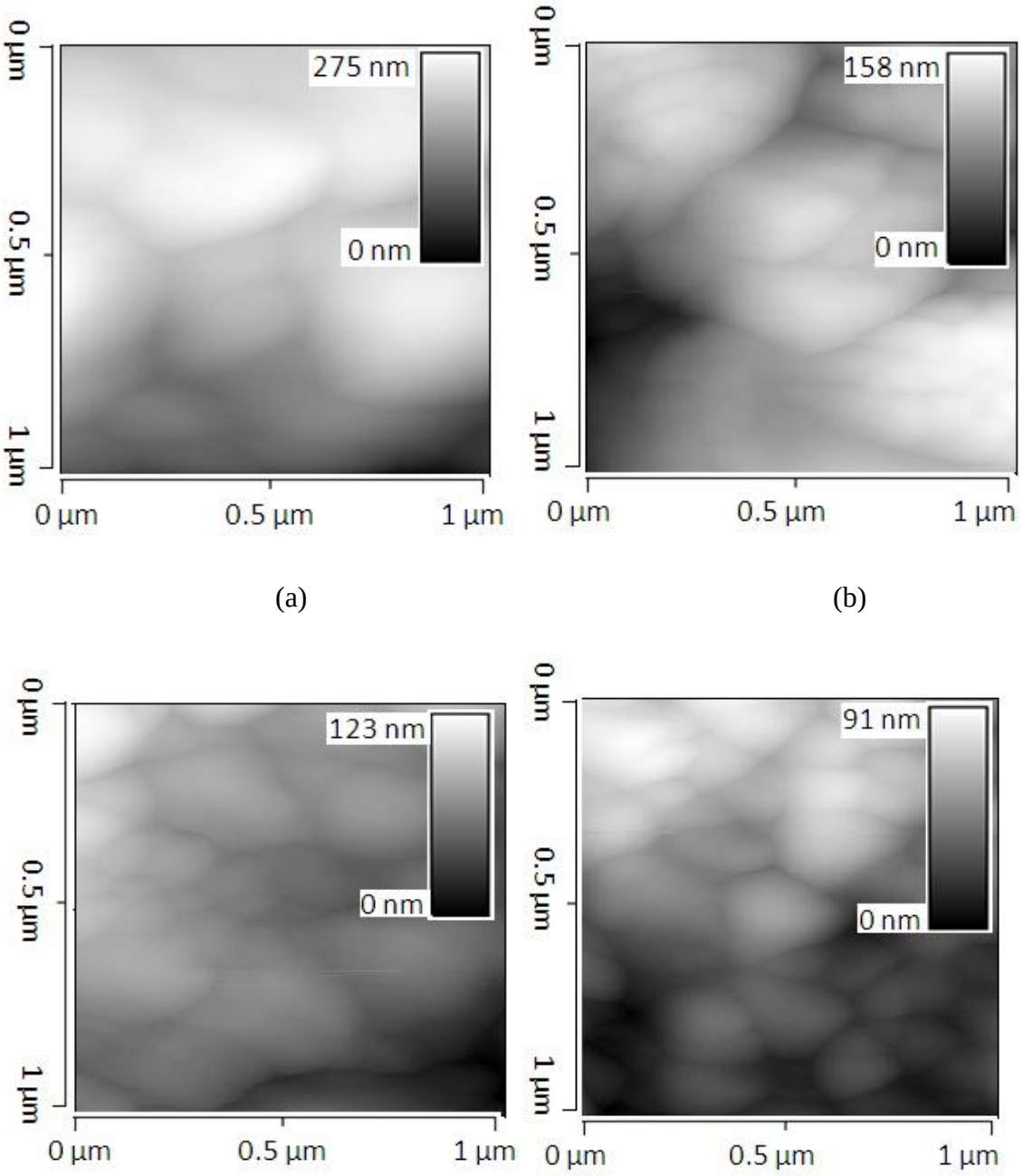

Figure 3.3 AFM micrographs of sonicated Cu deposits

for (a)5 s, (b)10 s, (c)15 s and (d) 20 s

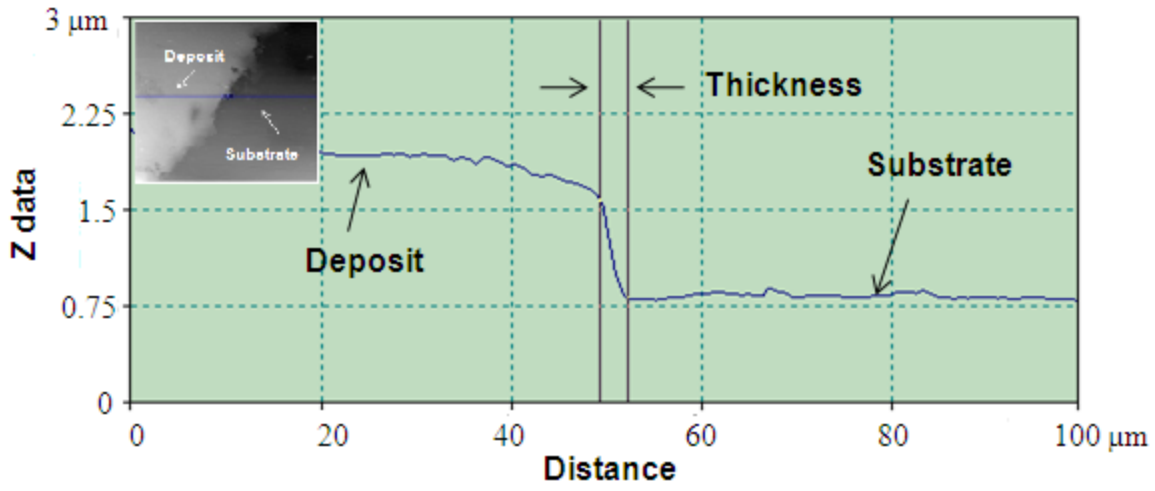

Figure 3.4 AFM micrograph of sonicated deposit at 20 s (Thickness measurement)

3.3 Electrochemical analysis

3.3.1 Chronoamperometry

Figure 3.5-3.7 shows the series of current transients (CT) for copper deposition with different operating parameters. The varying acid concentration effect is shown in Fig 3.5. From Fig. 3.5(a) it can be clearly seen that the shape of the silent current transients changes as the acid concentration is stepped to increasingly more concentration values. At low acid concentration values, the transients exhibit a sharp drop in current density followed by shallow current densities which have been assigned to adsorption and diffusion controlled growth processes respectively. Such an observation is in agreement with deposition studies observed by [54]. In contrast, at more acid concentration values, the initial sharp decay that is observed immediately after the potential decay is followed by a rising section at 40 and 50 gpl. This rising section appears to reach its maximum at increasingly shorter times with more acid concentration steps. The maximum in the current transients at high acid concentrations and short times corresponds to maximum surface area i.e. the point at which hemi-spherical nuclei are on the point of collision. Following this rising section of transient, a period of slow current decay occurs. It is also clearly visible that the current decay after rising portion does not decay fully, approaching a value of zero. One possible explanation for this could arise from the fact that hydrogen could have evolutes and, therefore, the value of current density after a sufficiently long period is due in part of the evolution of hydrogen.

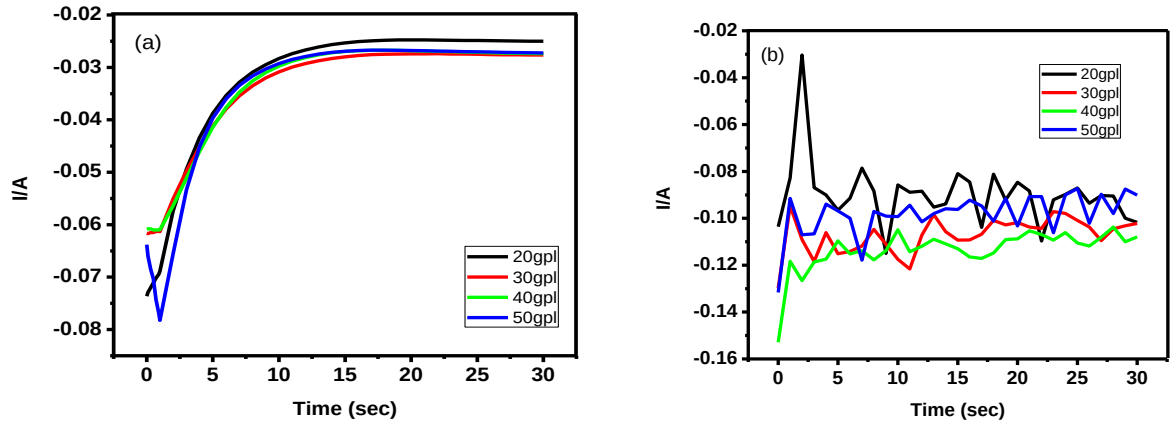

Figure 3.5: Choronoamperometri curves for the nucleation of copper at different acid concentrations under (a) silent and (b) sonication

The fact can be confirmed from the micrographs obtained under SEM and AFM as discussed in next section. A second possibility may be that the

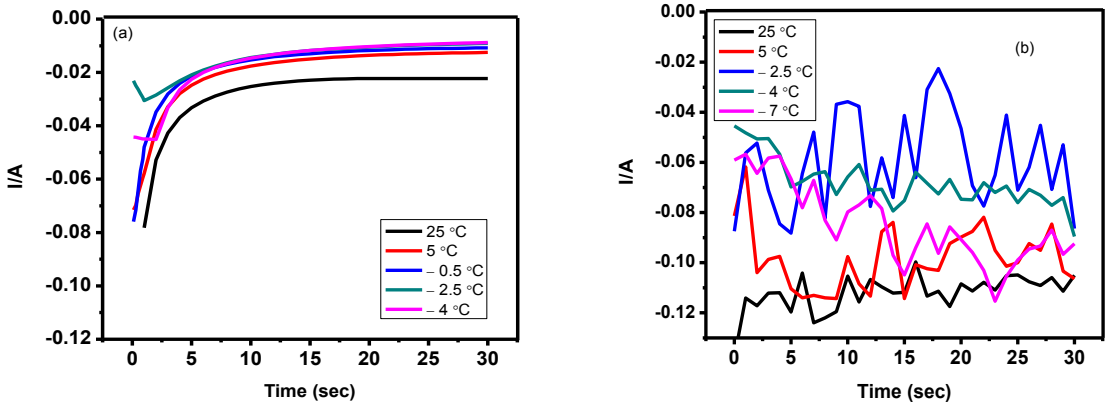

Figure 3.6: Choronoamperometric curves for the nucleation of copper at different temperatures under (a) silent and (b) sonication

consumption of copper and its subsequent replenishment at the electrode surface may be sufficiently rapid that the current decay may be retarded [55]. It is interesting to note that the expected $t^{-1/2}$ asymptote at long times is observed only at low acid concentrations at a rate that is proportional to the surface area of deposited copper. Consequently, hydrogen evolution dominates at high H^+ ion concentrations. Attention now turns to the affect that sonication has on

the deposition mechanism of copper. Fig. 3.5(b) shows the series of current transients for sonication for varying acid concentration. The transients have the typical shape as discussed in section 3.2. At 20 gpl the current maximum is around 110 mA, 1.5 times higher than the value of 65 mA at silent condition. The current maximums at all acid concentrations were higher than their corresponding silent experiments. The observed current is expected to result from the convolution of the nucleation and growth rates. The complication may be cleared from the morphological analysis, as discussed in the surface characterization section. Figure 3.6(a) shows current transients for copper deposits at low temperatures. The effect of supersaturation can easily be observed from the transients. At low temperatures the transients change from rapid decay of current to the typical nucleation and growth

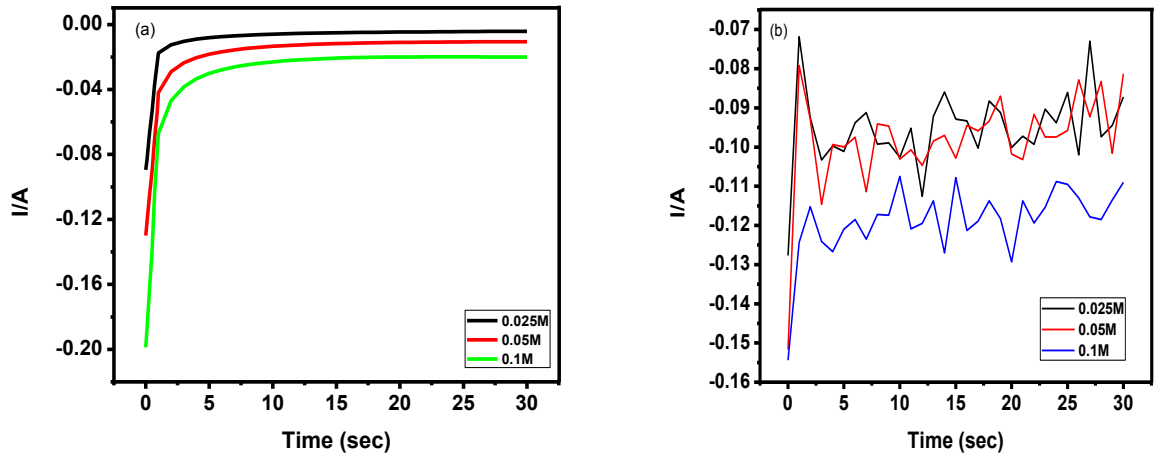

Figure 3.7 Choronoamperometri curves for the nucleation of copper at different copper concentrations under (a) silent and (b) sonication

of deposits at conducting surfaces. However, the transients exhibit rapid increase to a current peak that, in contrast to the solution of varying acid concentrations. The current transients for deposition in varying copper concentrations are shown in Fig. 3.7(a). The maximum in the Cu ion reduction current, I_{max} (plotted in fig 3.7 as negative) increases in magnitude as the Cu concentration is stepped to increasing values. At times longer than that corresponding to the current maximum (t_{max}), the reduction current decay follows the Cottrell behavior. At longer times, the current decreases rapidly, however the curves do not converge, as would be expected

for diffusion controlled growth. In contrast to the transients shown in Fig. 3.5(a) and 3.6(a), the current decay after the maximum remains large even at more positive potentials.

3.3.2 Nucleation and growth models

The current transients shown in Fig. 3.5-3.7 are presented again in Fig. 3.8 respectively, in dimensionless form and compared to the theoretical transients. The theoretical curves for progressive and instantaneous nucleation diffusion-limited growth are also shown.

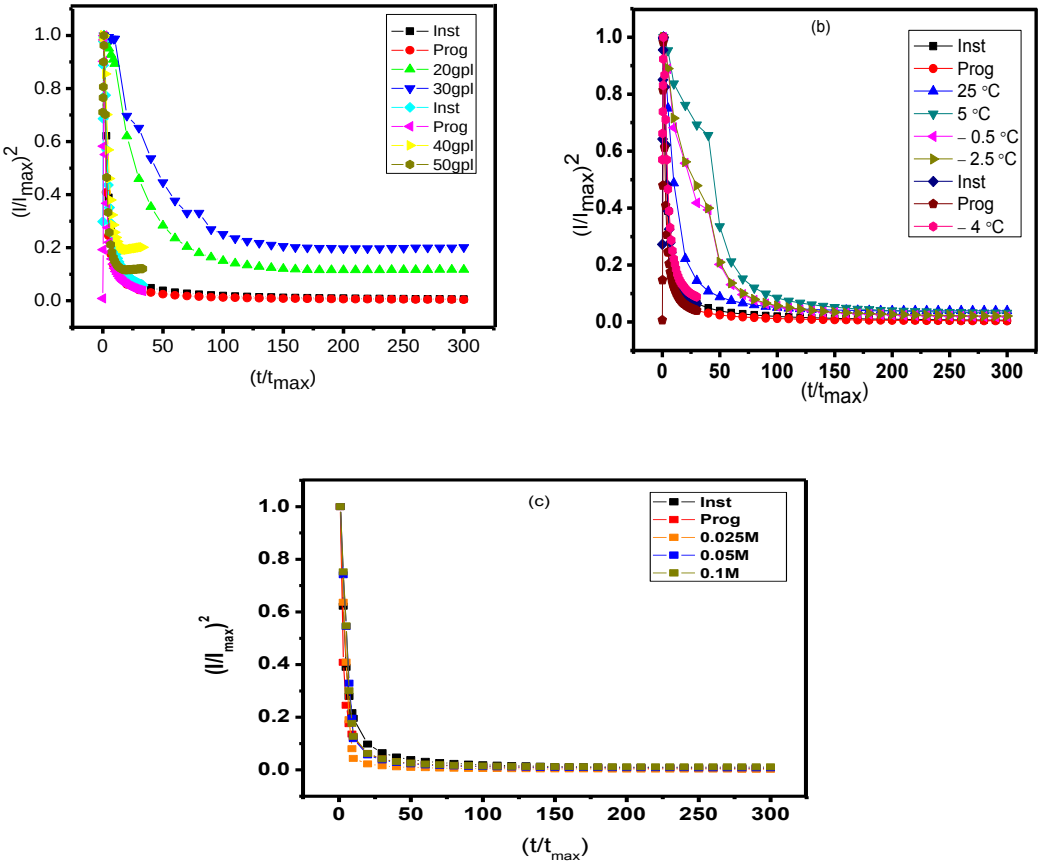

Figure 3.8: $(I/I_{max})^2$ vs. (t/t_{max}) analysis of CTTs for Cu with the data for the theoretical instantaneous and progressive nucleation modes for varying (a) acid concentrations, (b) temperatures and (c) Cu concentrations

The experimental data are compared to the "Scharifker-Hills" model behavior. According to Fig. 3.8 corresponding to acid concentration, it is apparent that copper follows progressive nucleation

mode in increasing acid concentration. Neither the instantaneous nor progressive model does provide an adequate description of the kinetic data at low acid concentration.

Table 3.4: Quantity of charge passed and measured thickness at different operating parameters

Acid Conc. (gpl)	**Charge (C)**		**Film Thickness (nm)**	
	Silent	Sonication	Silent	Sonication
20	0.944	2.68	155.4	441.2
30	0.997	3.21	164.2	528.5
40	0.982	3.38	161.7	556.5
50	1.000	2.93	164.6	482.4
Copper Conc. (M)	**Charge (C)**		**Film Thickness**	
	Silent	Sonication	Silent	Sonication
0.025	0.227	2.53	37.4	416.5
0.050	0.492	2.93	81.0	482.4
0.100	0.838	3.55	137.9	584.5
Temperature	**Charge(C)**		**Film thickness (nm)**	
	Silent	Sonication	Silent	Sonication
25°C	0.882	3.35	145.2	551.5
5°C	0.593	2.96	97.6	487.3
−0.5°C	0.510	1.75	83.9	288.1
−2.5°C	0.518	2.04	85.3	335.9
−4.0°C	0.433	2.55	71.3	419.8

Hence the plateau should follow the progressive 3D nucleation and so the result. An attempt has been made to calculate the thickness according to the equation 3.1. The measured quantity of charge passed and the calculated film thickness are presented in Table 3.4. The film thicknesses fall in the range of 400-500 nm. In a varying acid field, thickness increases so as with copper concentrations also. However with temperature thickness values do not follow any trend and lie have more or less same values.

3.4 Surface Characterization

3.4.1 Phase analysis

X-ray diffraction was used to characterize the copper surface. Figure 3.9 shows the spectrum for the copper deposits for sonicated samples at varying acid concentrations, temperature and copper concentrations respectively. It is indicated that the dominant diffraction peaks of FCC Cu-Zn (ICDD 25-1228) and brass (ICDD: 50-1333) [56, 57] are clearly observed. Three main peaks at 2θ = 43.266°, 72.127° and 79.291° are attributed to the (330), (631) and (720) planes with (330) being the most intense are detected. As the film thickness are below 1 µm, the X-ray beams might have penetrated to the surface more pass the coating resulting the Cu-Zn compound identification and not the pure copper.

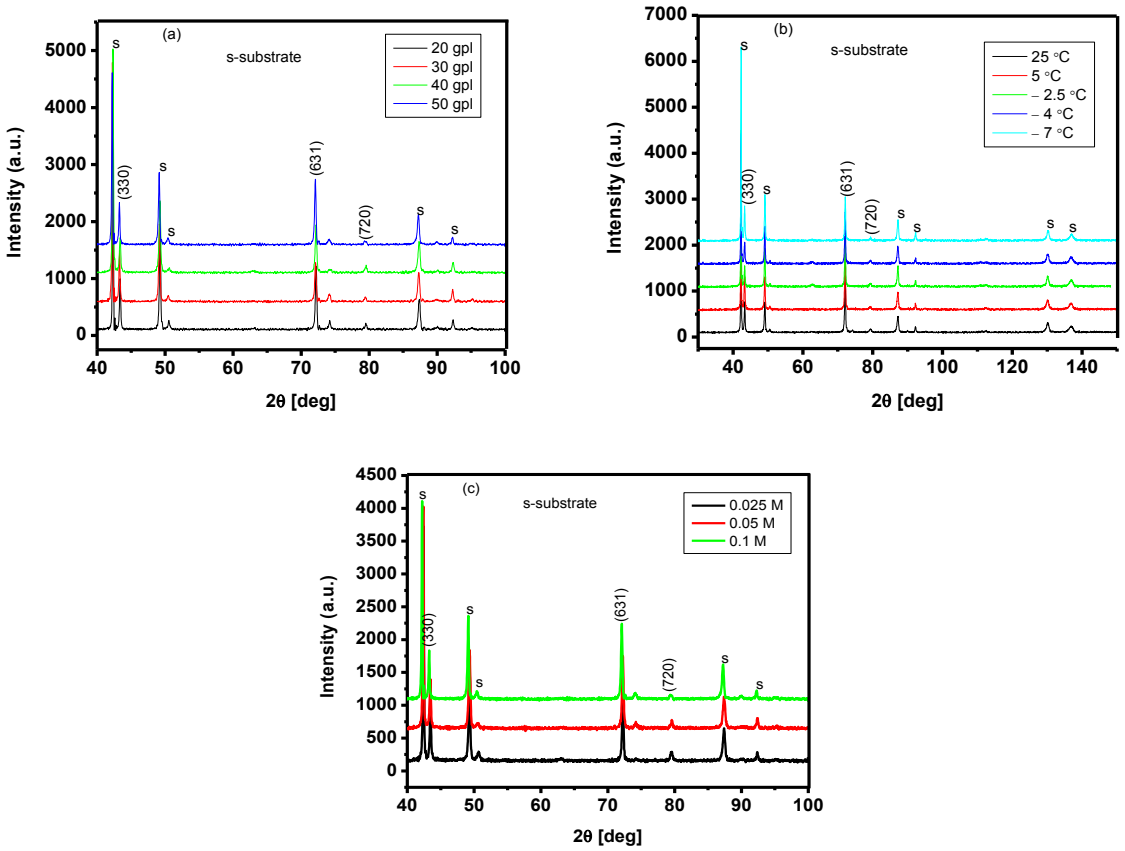

Figure 3.9 : The XRD pattern for the Cu films deposited at varying (a) acid concentrations, (b) temperatures and (c) Cu concentrations

3.4.2 Structural analysis

Fig. 3.10 shows the SEM micrographs for the films deposited at various acid concentrations in silent conditions. It was found that acid concentration strongly affects the density of Cu nuclei, their size and the surface coverage. The images display that there is good surface coverage. Fig.3.10(d) shows that the films deposited at 50 gpl acid concentrations comprises hole like irregularities covering the surface. The effect of hydrogen evolution on the formation of a very open, porous and disperse structure of copper can be easily analyzed from

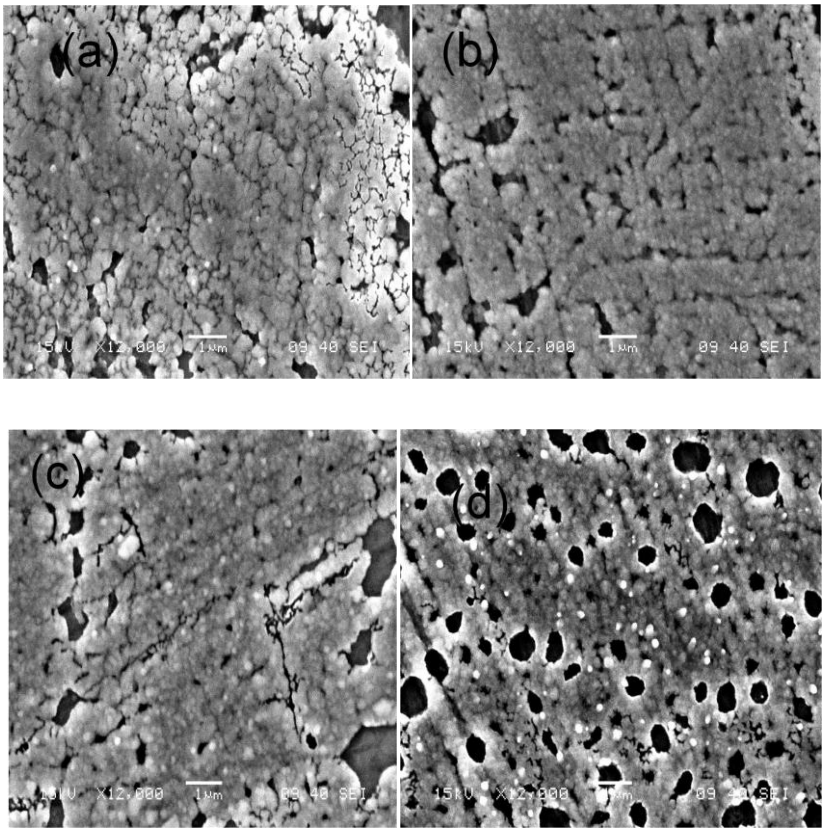

Figure 3.10: SEM photograph of silent deposit at magnification ×12000 for different acid concentration (a) 20gpl, (b) 30gpl, (c) 40gpl, (d) 50gpl

the Figure 3.10. At this acid concentration hydrogen evolution was more vigorous than the low values. The corresponding morphological analysis of deposits under sonication is given in Fig 3.11. A complete coverage of the substrate can be observed from the figure. However, the deposits posses traces of polishing lines (long range scratches due to the polishing procedure), indicating that the copper layer is not thicker than approximately 0.5 μm. In the case of a complete coverage of the

surfaces, the electrodeposition of Cu follows two different mechanisms. Firstly, the deposition occurs on the bare neatly prepared brass surface, by in-situ cleaning of the electrodes by ultrasound. In the initial stage copper is deposited preferentially on the surface steps and on the defects of the brass substrate. Afterward, the nuclei population density increases and the Cu deposit expands on the totality of the surface. A continuous deposition of Cu occurs on the freshly deposited Cu particles. Secondly, the capability of ultrasound to absorb gases for the onset of cavitation phenomena may have removed all the hydrogen gas evolved from the surfaces. This process results in a smoother uniform surfaces as compared the coatings of the silent deposits. However, the SEM studies were not capable of producing the morphological details. Hence the structural characteristics are further ventured with AFM. Wide area (2 μm × 2μm) AFM scans of the acid concentrations are shown in Fig 3.12 for freshly prepared copper deposits.

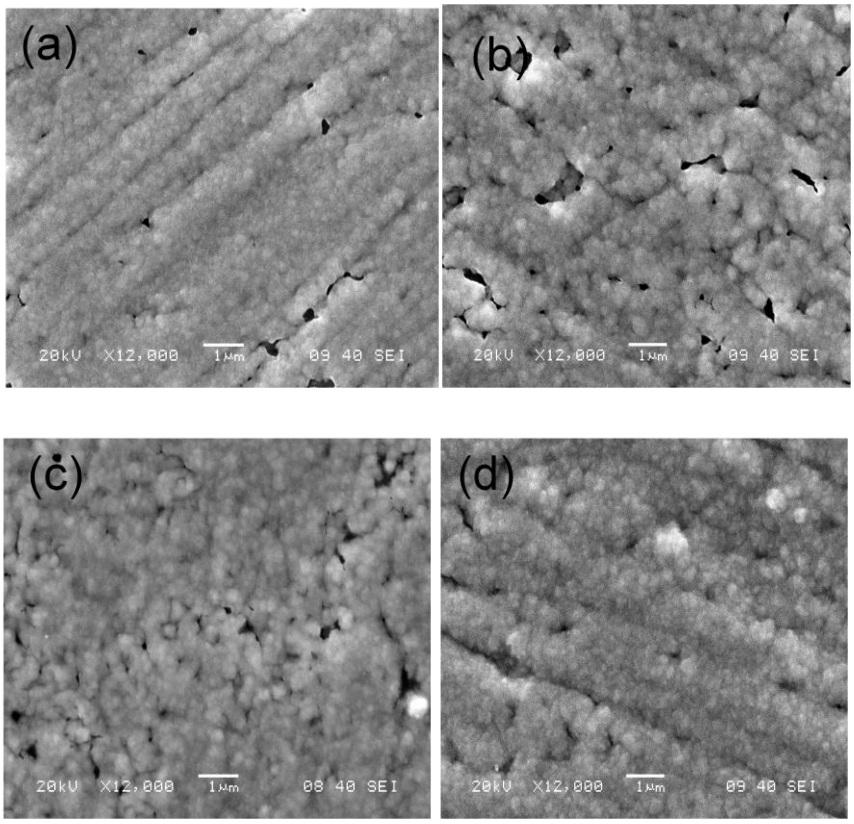

Figure 3.11: SEM photograph of sonicated copper deposits at magnification ×12000 for different acid concentration (a) 20gpl, (b) 30gpl, (c) 40gpl, (d) 50gpl

An increase in uniformity and smoothness of the surfaces morphology with acid can clearly be observed. The roughness of the crystals at 20 gpl is 106 nm and the maximum height is around 477 nm. The surface details and the average roughness factors are given in Table 3.5.

Table 3.5: Roughness factors of Cu deposits for different operating parameters

Acid Conc. (gpl)	R_a* (nm)	Temperature (°C)	R_a (nm)	Cu conc. (M)	R_a (nm)
20	106	**25**	300	**0.025**	36
30	100	**5**	170	**0.05**	67
40	59	**–0.5**	71	**0.1**	128
50	33	**–2.5**	35	-	-
-	-	**–4**	14	-	-

*R_a = Roughness factor

The data indicates the smoothness of the surfaces with increasing acid concentrations, as the roughness of 50 gpl acid is only 33 nm compared to values of 59 and 100 nm for 40 and 30 gpl respectively. The grains at 40 and 50 gpl have not noteworthy change in overall height.

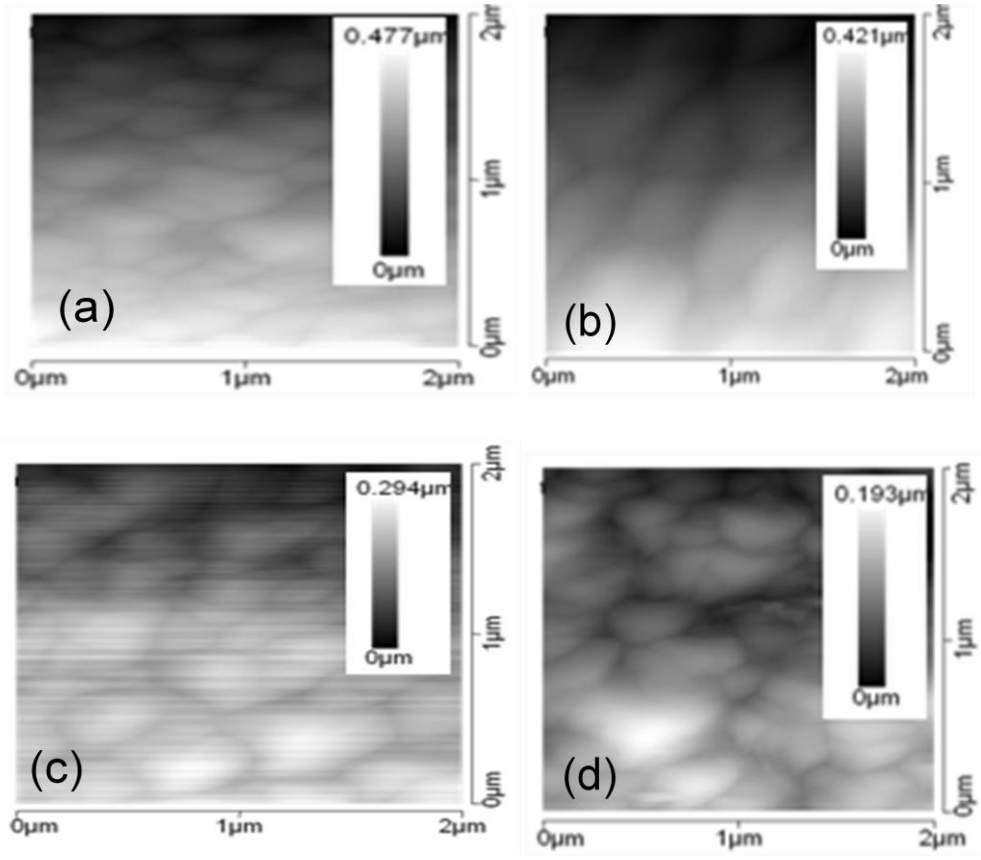

Figure 3.12 AFM micrograph of sonicated deposit for different acid concentration (a) 20gpl, (b) 30gpl, (c) 40gpl, (d) 50gpl

This may be an evidence that lateral growth proceeds more quickly than vertical under these conditions. There are hardly any significant changes from low acid values to high acid values. The deposits at 20 and 30 gpl seem to have the grains in single size range. At 40 and 50 gpl, among the large copper nuclei, a notable presence of small grains can be observed. The kinetic data (Fig 3.8) indicate that the mode of nucleation changes significantly with acid concentration. At high acid values, the nucleation is described well by the model of progressive nucleation. The slow and continuous appearance of active sites (progressive) might have caused the above results. Thus, increased acid concentration values were responsible for the grain height decrease, as well as the increase of regularity, and the increase of surface nuclei population density.

The structural difference by morphological studies between the investigated coating systems at varying temperatures for both silent and ultrasonic conditions can be detected from Fig 3.13 and 3.14. The application of ultrasound was found to affect the rate and mechanism of Cu deposition, and also the morphological detail of the deposits. The SEM images under sonication display that there is good surface coverage, good crystallinity and no crack in the surfaces of the films. Fig 3.14 shows that the film deposited at – 4 °C comprises of better uniform grain size and surface finish (micro rough) while at 25 °C deposits are much more rough and non-uniform. The deposit at – 4 °C posses traces of polishing lines also. A highly adherent deposit in ultrasonic conditions can also be observed. However the deposits without sonication shows smaller grains and the population density has decreased at low temperatures as evident by the poor surface coverage. The shape and size of the grains of the sonicated copper samples are further analyzed by AFM studies as shown in Fig 3.15.

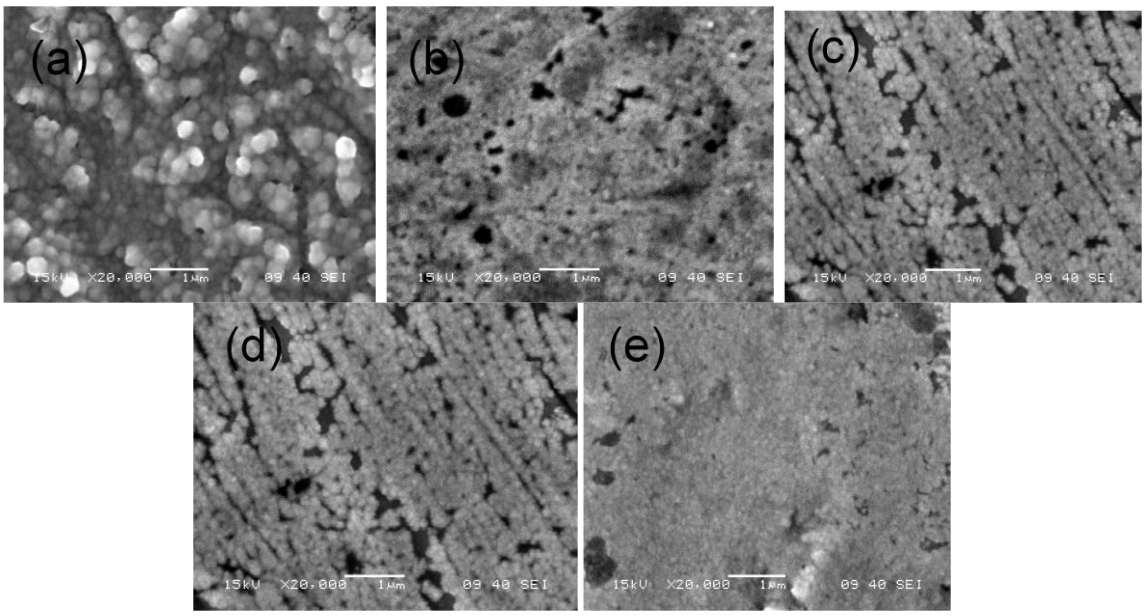

Figure 3.13: SEM photograph of silent deposit at magnification ×20000 for different bath temperature (a) 25^0C, (b) 5^0C, (c) -0.5^0C, (d) -2.5^0C, (e) -4^0C

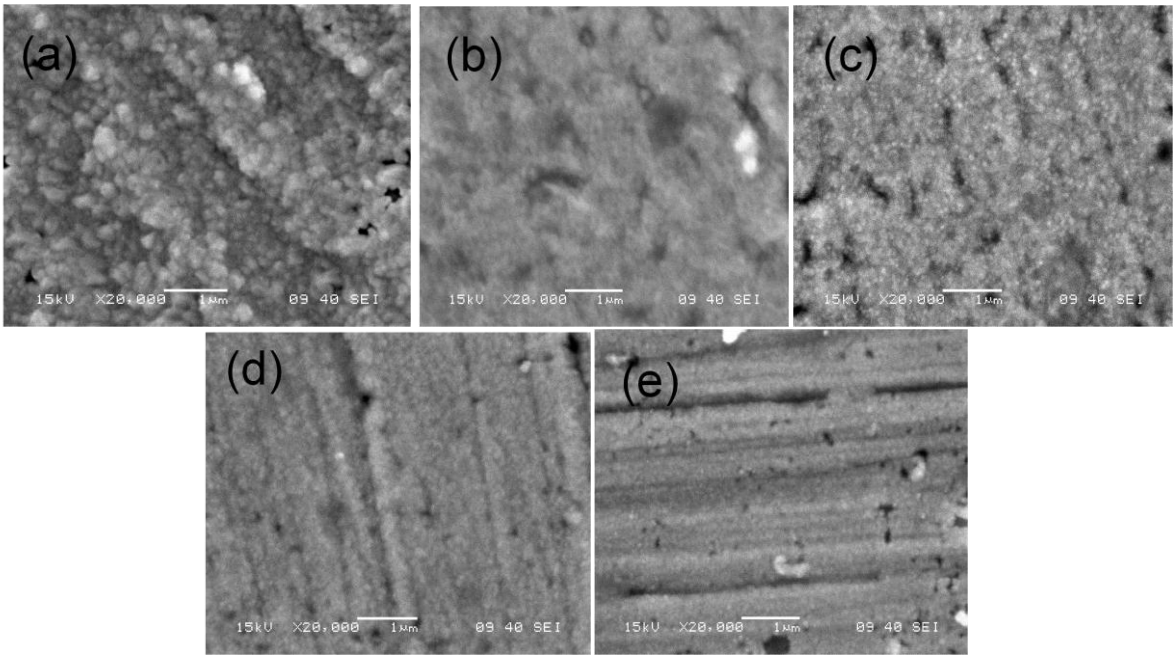

Figure 3.14 SEM photograph of sonicated deposit at magnification ×20000 for different bath temperature (a) 25^0C, (b) 5^0C, (c) -0.5^0C, (d) -2.5^0C, (e) -4^0C

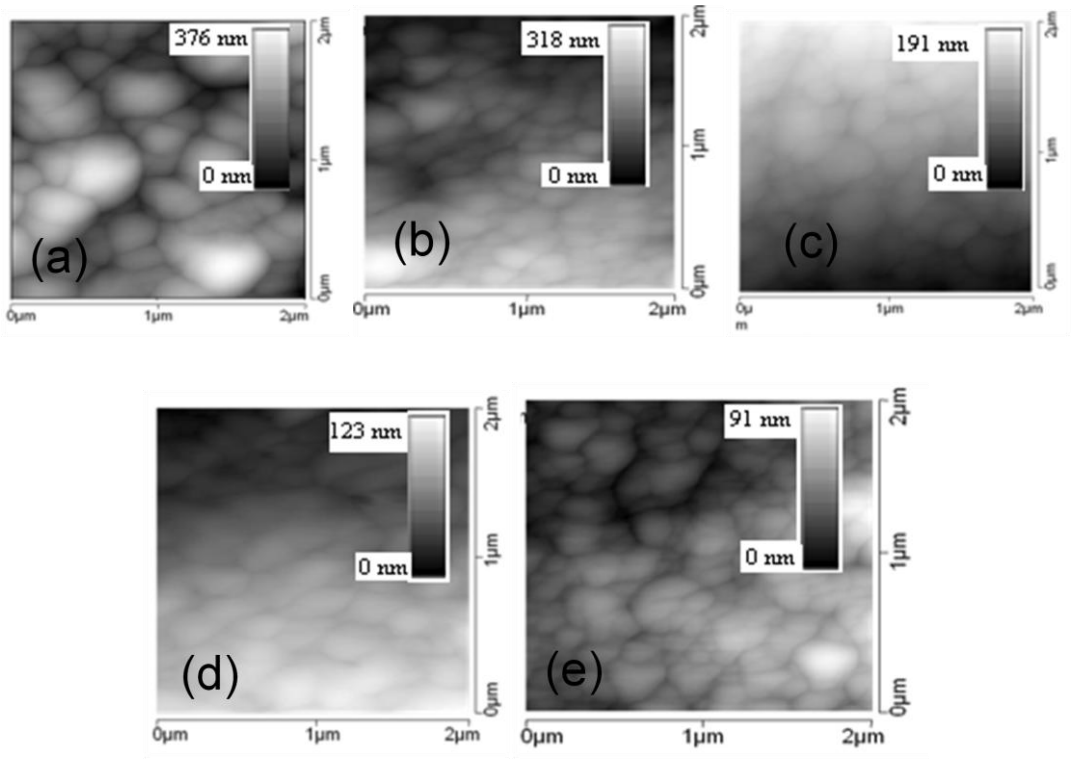

Figure 3.15 : AFM micrograph of sonicated deposit for different bath temperature (a) 25^0C, (b) 5^0C, (c) -0.5^0C, (d) -2.5^0C, (e) -4^0C

The grains appear to be hemi-spherical or nearly spherical and highly agglomerated. The mode of agglomeration prevents the analysis and calcualtion of the size of the crystals. However, the maximum grains of deposit at 25 °C are in the size range of 200-400 nm with a maximum height of 376 nm and average roghness of 300 nm. The complete analysis of the deposits are given in Table 3.5.The above effects of ultrasound in a highly supersaturated parent phase (low temperature) is based on the following facts. Low temperature favors nucleation ahead of growth (details discussed in chapter 1). Ultrasound generally increased the rate of deposition, as anlyzed by CV and CCT, except at small tip-electrode separations, where ablation was found to be a dominant factor. As such the increase in current under ultrasonic agitation might arise from the enhanced nucleation, enhanced growth or both. It has been mentioned by Floate et. al. that ultrasound affects growth rather nucleation [53]. However, we have observed the impact on both nucleation and growth and are far from conclusion. The application of ultrasound favors a more instantaneous nucleation behavior at all operating conditions. Such observations of changes to the nucleation behavior may result from an ablation effect of ultrasonic agitation that strips away newly formed/poorly adhering nuclei from the

electrode surface and combined with the secondary nucleation on existing nuclei might result in fine grained adherent deposits at low temperatures.

Fig 3.16 represents the results from the copper deposition study 0.1, 0.05 and 0.025 M Cu^{2+} solutions. The deposit at 0.1 M is relatively small, uniform and densely distributed on the surface. At low copper concentration, the size of nuclei increased, but the nuclei population density decreased, which is even more pronounced at a lower copper concentration, Fig 3.16. The results may be explained in the following ways. At the very beginning of electroreduction the number of copper atoms produced on the surface is a function of initial bulk concentration. In the case of low metal ion concentration the Cu atoms are spaced further apart compared with the case of high metal concentration. Once distributed over the surface in the atomic state, atoms must travel towards each other in order to minimize surface energy. Atoms spaced longer apart have to travel long distance to form the nucleus. Since this is energetically unfavorable they have to group together with the neighbor atoms to from large number of small nuclei. On the other hand, when the initial concentration is very high, the close proximity of atoms will result in grouping to form a large nucleus. However the fact that ultrasound capable of crystal breakage may further affect the nucleation mechanism, resulting the concept of secondary nucleation phenomena. The big grains at high Cu concentrations are broken and nucleation has occurred on the primary nuclei. The effect will be more pronounced with the availability of nuclei centers for secondary nucleation. Hence the deposit at higher concentration should be finer. However the heighted crystals at 0.1 M do fall at a value of 1.564 μm. The height as well as roughness factors also reduce at still low concentrations. The most availability of ions at higher concentrations might have caused the above results.

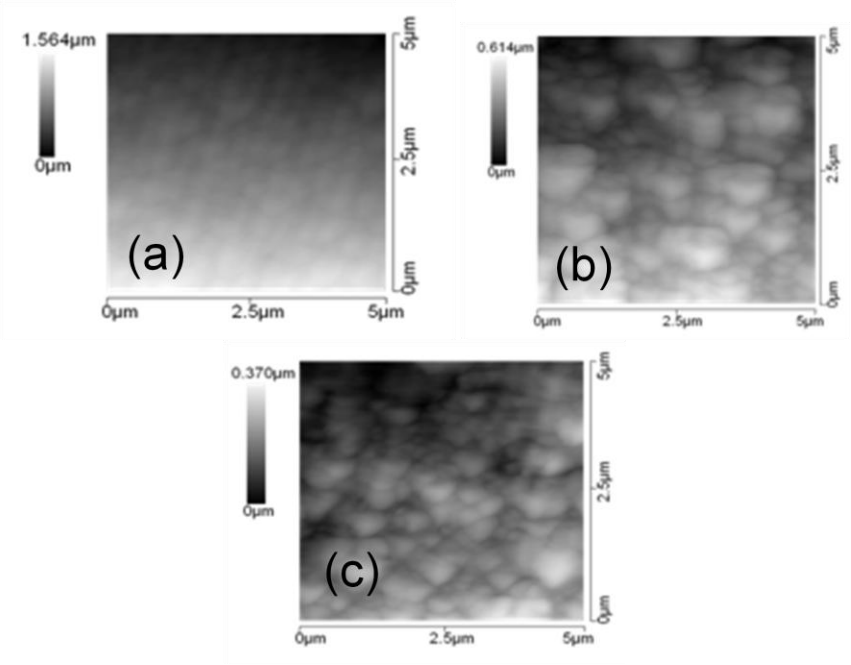

Figure 3.16: AFM micrograph of sonicated deposit for different copper concentration (a) 0.1M, (b) 0.05M, (c) 0.025M

3.5 Hardness characteristics

3.5.1 Effect of bath temperature on hardness of copper thin film

Nanoindentation tests were conducted with a Berkovich diamond indenter using the load-displacement sequence. The load vs. displacement curve was measured for all the samples. Typical plots obtained for samples, deposited at different bath temperature, are shown in figure (3.17). After initial contact of the indenter on surface, the load was increased at a predetermined rate to the desired maximum load and then decreased at the same rate to zero. The unloading curve followed the partial elastic recovery of the sample material. From this plot the hardness (*H*) and the elastic modulus (*E*) were calculated. The indentation load-displacement data obtained at each depth was analyzed to determine the hardness using the method of Oliver and Pharr, according to the relation:

$$H = \frac{P_{max}}{A} \qquad (3.2)$$

where $P_{\max}$ is the peak indentation load and A the indentation contact area, which was determined from the indenter shape function. In general, the loading data are influenced more by

the plastic properties of the material and unloading data by the elastic properties. The hardness values were calculated from the loading portion of the curves.

Table 3.6: Hardness of deposits at different bath temperature

Bath Temperature (°C)	Hardness (GPa)
25	1.6512
5	1.8612
– 0.5	1.9831
– 2.5	2.4519
– 4	2.5459

In general, the hardness values measured by nanoindentation are sensitive functions of the surface roughness, oxidation of the surface layer and indenter size effect. [58]

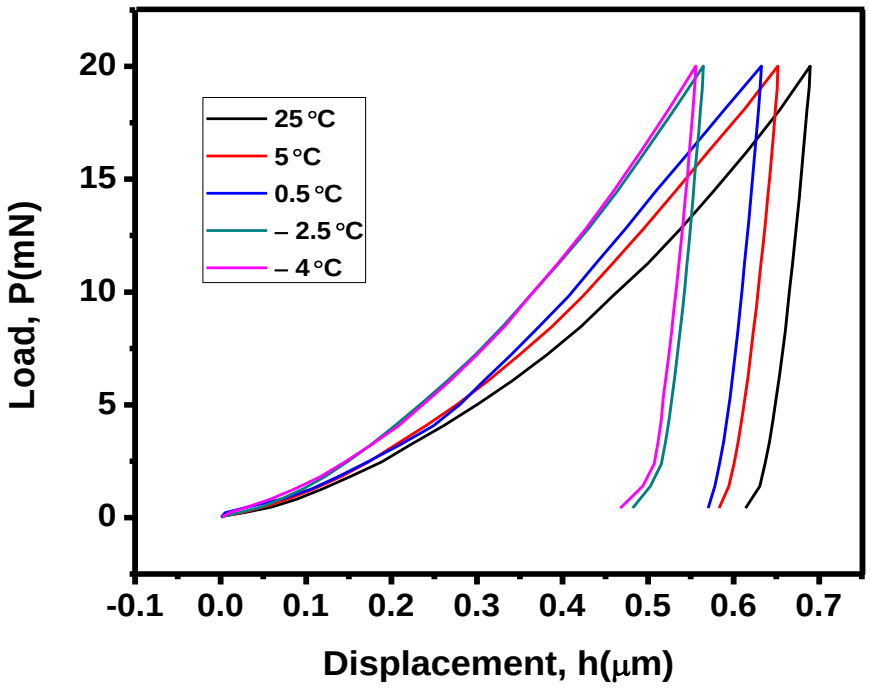

Fig 3.17: Load-displacement curve for deposits, deposited at various temperature

Figure (3.17) shows the hardness characteristics of the deposit, deposited at various bath temperatures in the presence of ultrasound. The tests are done with a constant load applied to the substrate and the displacement is recorded for each of the temperatures. The applied load was 20

mN for the nanoindentation measurements. For this load the maximum penetration depth may be higher than the coating thickness. Therefore, the measurements may affected by the nature of the substrate. But the substrate is same for all the samples so the change in measurements may be due to the change is hardness of thin film. It can be seen that the displacement decreases with decreasing temperature. The conventional Hall-Petch equation, hardness/yield strength increases as

$$H = H_0 + kd^{-1/2} \qquad (3.3)$$

is followed from the above observation. The fact can be explained as dislocation which moves from one grain into another has to adjust its direction with increasing number of grain boundaries. Thus it can be inferred that the more grains a material has, the more difficult for the dislocations to move. To put it in another way, the finer the grains are, the harder the material is.

3.5.2 Effect of acid concentration on hardness of copper thin film

Figure (3.18) shows the hardness characteristics of the deposit, deposited at various acid concentration in bath in the presence of ultrasound. The tests were done with a constant load applied to the substrate and the displacement is recorded for each sample. The applied load was 20 mN for the nanoindentation measurements. For this load the maximum penetration depth may be higher than the coating thickness. Therefore, the measurements may affected by the nature of the substrate. But the substrate is same for all the samples so the change in measurements may be due to the change is hardness of thin film. It can be seen that the displacement decreases with increasing acid concentration of electrolytic bath.

Table 3.7 Hardness of deposits at different acid concentration

Acid concentration	Hardness (GPa)
20 gpl	1.798
30 gpl	1.9015
40 gpl	1.7758
50 gpl	2.0034

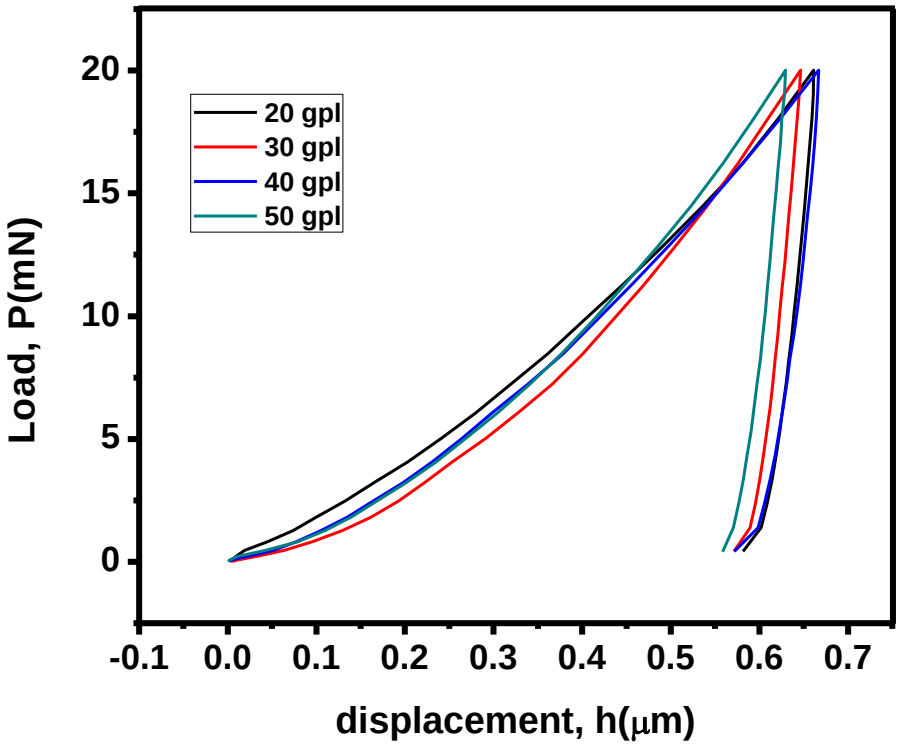

Fig (3.18): Load-Displacement curve for different acid concentration

With increasing acid concentration in electrolytic bath, the grain size will reduce and the numbers of grain will increase on the substrate. The fact can be explained as dislocation which moves from one grain into another has to adjust its direction with increasing number of grain boundaries. Thus more grains a material has the more difficult for the dislocations to move. Hardness of the film will increase with increasing acid concentration in electrolytic bath due to small grain deposit deposited on substrate.

3.5.3 Effect of copper concentration on hardness of copper thin film

The influence of concentration on the rate of nucleus formation is uncertain; since increase of concentration tends to give firm, adherent deposits, some workers have expressed the opinion that the presence of the large number of ions in a concentrated solution favors the growth phase than the nuclei formation mechanism.

Table 3.8: Hardness value of deposits at different copper concentration

Copper Concentration	Hardness (GPa)
0.1M	1.354
0.050M	1.8683
0.025M	1.9708

However we have observed harder film at higher copper concentrations which complements the results obtained from morphological analysis.

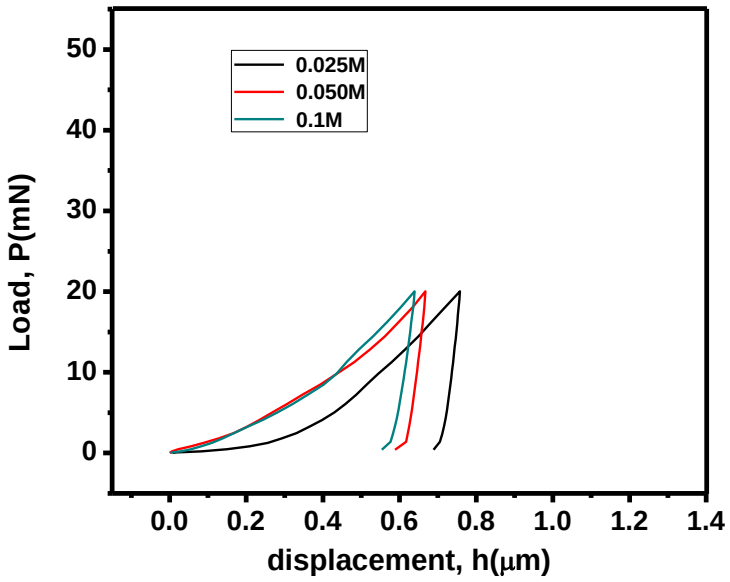

Figure 3.19: Load displacement curve for deposits, deposited at different copper concentration

CONCLUSIONS

Copper films were cathodically electrodeposited in an ultrasonic field on oxygen free brass substrates from an aqueous solution containing H_2SO_4 and $Cu_2SO_4.5H_2O$ by changing the acid concentration, reaction temperature and copper ion concentration at a single step potential. The deposit films were characterized with X-ray diffractograms, microstructure analysis by SEM and AFM and hardness studies by nanoindentation.

The observations and analysis of the results obtained from the above studies are enlisted as follows:

1. Cyclic voltammetry (CV) was performed in the [0.8 to –0.6] V potential range to identify the presence of the electrodeposition processes and to verify the electrochemical behavior of the electrodes in the electrodeposition bath with and without ultrasound. The cathodic and anodic peaks are observed at –0.083 & –0.261 and 0.183 & 0.479 V for silent and sonication conditions respectively. The sonication current observed is three times higher than that of silent conditions, indicated the enhanced mass transport by ultrasound. A potential of 450 mV (100 mV negative than the Nernst potential) was selected for the deposition procedure for all the conditions.
2. The sole impact of sonication was experimented before the study of the coupling effect. The comparison with the Scharifker and Hills limiting cases indicate that at longer period of deposition, crystal breakage leads to higher population density. However the proposed phenomena may not proceed for infinite period of time due to increased adherence under sonication. Contact mode AFM was used to confirm the conclusions drawn from the CCTs and the morphologies observed agreed well with those expected. We believe that the major significance of this better insight is the opening up of new possibilities for the use of sonoelectrochemical synthesis for electronic industries to solve the problem of superfilling.
3. Chronoamperometric curves and theoretical instantaneous and progressive curves were used to study the synthesis mechanisms and kinetics. The thickness of films lies in the range of 400-500 nm. The nucleation population density got increased from a low value to high value of acid concentrations. The evidence of secondary nucleation in ultrasonic condition was also observed. Comparison with the theoretical models, it is apparent that

copper follows progressive nucleation mode in increasing acid concentration. Neither the instantaneous or progressive model does provide an adequate description of the kinetic data at low acid concentration. And insonation stick to the regime of instantaneous nucleation for the primary nuclei loop. Hydrogen evolution was also imperative at increasing acid concentrations, however, ultrasound capable of degassing produced hydrogen free adherent surfaces. The facts are also confirmed by the morphological analysis by SEM and AFM. Roughness study by AFM confirms smoother deposits with acid concentrations. The roughness value decreased from 106-33 nm for the values of 20-50 gpl acid respectively. Hardness values (1.7-2.0 GPa) also support the results obtained by CTTs and morphological analysis.

4. The same trend is observed for the films with low temperatures, however hydrogen evolution were not prominent during the deposition. The average roughness varied from 300-14 nm. The above result follows the fact that high supersaturation along with the triggered localized supersaturation of ultrasound has elevated the nucleation ahead of growth. Among all the depositions copper films at – 4 °C is the smoothest. The hardness values varied from 1.6-2.54 GPa.
5. Increasing metal ion concentrations produces finer and harder deposits. These results however, do not agree with the literatures available and are explained on the basis of secondary nucleation induced by crystal breakage in an ultrasonic field. Films are more rough at 0.1 M as compared to that of 0.025 M. This result is supported by the fact that crystal formations on the existing crystals (the phenomena of secondary nucleation) have formed heighted particles than the deposits at low copper concentrations where the availability of crystals is less. 1.3-1.9 GPa of hardness values are measured under the indenter.
6. The phases of the deposits are confirmed by the XRD analysis. It is indicated that the dominant diffraction peaks of FCC Cu-Zn (ICDD 25-1228) and brass (ICDD: 50-1333) are clearly observed. Three main peaks at $2\theta = 43.266°$, 72.127° and 79.291° are attributed to the (330), (631) and (720) planes with (330) being the most intense are detected. As the film thickness are below 1 µm, the X-ray beams might have penetrated to the surface more pass the coating resulting the Cu-Zn compound identification and not the pure copper.

In summary, electrodeposition methodology under sonication presented in this work appear to be efficient to produce good quality metal films with special properties and thus has the potential of being exploited for both research purposes and industrial applications.

REFERENCES

1. Chopra K. L., Kaur I.; *Thin film Device applications*; New York and Plenum Press, 1983.
2. Garg A.; *Growth and Charaterization of Epitaxial oxide Thin Films*; Doctoral dissertation, St. John's college, University of Cambridge, 2001.
3. Venables J. A., Spiller G.D.T., and Hanbucken M.; *Nucleation and Growth of Thin Films*; Report on Progress in Physics, 47 (1984): pp. 399-459.
4. *Modification of thin film properties by sputtered particles*; R & D Review of Toyota CRDL, 28 (1993).
5. Bicelli L. P., Bozzini B., Mele C., D'Urzo L.; *A review of nanostructured aspects of metal electrodeposition*; International Journal of Electrochemical Science, 3 (2008), pp 356-408.
6. Paunovic M., Schlesinger M.; *Fundamental of electrochemical deposition second edition*. John Wiley & sons, U.S.A. 2006.
7. Eskhult J.; *Electrochemical deposition of nanostructured metal/metal oxide coatings*; Doctoral dissertation, Acta Universitatis Upsaliensis Uppsala, 2007.
8. Budevski E., Staikov G., Lorenz W.L.; *Electrocrystallization: Nucleation and Growth Phenomena*; Electrochimica Acta, 45 (2000): pp. 2559-2574.
9. Staikov G., Milchev A., Staikov G. (editor); *Electrocrystallization of Nanotechnology*; Wiley VCH Weinheim, 2007.
10. Schultze J.W, Heidelberg A, Rosenkranz C, Schapers T, Staikov G.; *Principle of electrochemical nanotechnology and their applications in materials and systems*; Electrochimica Acta, 51 (2005): pp 775-786.
11. Zhang J., Chi Q., Albrecht T., Kuznetsov A. M, Grubb M., Hansen A. G., Wackerbarth H., Welinder A. C., Ulstrup J.; *Electrochemistry and bioelectrochemistry towards single molecule*; Electrochimica Acta, 50 (2005): pp 3149-3159.
12. Jason R. D.; *Electrochemistry in nanoparticle science*; Current Opinion in Colloid & interface Science, 7 (2002): pp 186-192.

13. Gomez H., Henriquez R., Schrebler R., Cordova R., Ramirez D., Riveros G. and Dalchiele E. A.; *Electrodeposition of CdTe thin films onto n-Si(100): nucleation and Growth mechanisms*. Electrochimica Acta, 50 (2005):pp 1299-1305
14. Hass I., Shanmugum S., and Gedanken A.; *Pulsed sonoelectrochemical synthesis of size controlled copper nanoparticles stabilized by poly (N-vinylpyrolidone)*; Journal of Physical Chemistry B, 110 (2006): pp 16947-16952.
15. Ghasemi S., Karami H., Mousavi M. F., Shamsipur M.; *Synthesis and morphological investigation of pulsed current formed nano structured lead dioxide*; Electrochemistry Communications, 7 (2005): pp 1257-1268.
16. Grujicic D., Pesic B.; *Electrodeposition of copper: the nucleation mechanism*; Electrochimica Acta, 47 (2002): pp 2901-2912.
17. Mahalingam T., Raja M., Thanikaikarasan S., Sanjeeviraja C., Velumani S., Moon Hosun, Kim Yong Deak; *Electrochemical deposition and characterization of Ni-P alloy thin films*; Materials Characterization, 58 (2007): pp 800-804.
18. Radovici O, Vass C., and Solacolu I; *Some aspects of copper electrodeposition from pyrophosphate electrolytes*; Electrodeposition and Surface treatment, 2 (1973/74): pp 263-273.
19. Natter N. and Hempelmann R.; *Nanocrystalline copper by pulse electrodeposition: The effect of organic additive, Bath temperature, and pH*; Journal of Physical Chemistry, 100 (1996): pp 19525-19532.
20. Nikolic N. D, Pavlovic L. J, Palvolic M. G, Popov K. I.; *Effect of temperature on electrodeposition of disperse copper deposits*; Journal of the Serbian Chemical Society, 72(12) (2007): pp1369-1381.
21. Mallik A, Ray B.C.; *Morphological study of electrodeposited copper under the influence of ultrasound and low temperature*; Thin Solid Films (2009), doi: 10.1016/j.tsf.2009.04.054.
22. Fenineche N. and Coddet C.; *Effect of electrodeposition parameters on the microstructure and mechanical properties of Co-Ni alloys*; Surface Coating Technology, 41 (1990): pp 75-81.

23. Seo M. H., Kim D. J., Kim J. S.; *The effect of pH and temperature on Ni-Co-P alloy electrodeposition from a sulphamate bath and the material properties of the deposits*; Thin Solid Films, 489 (2005): pp 122-129.
24. Kaischew R, Mutaftschiew B.; Bull. Acad. Bulg. Sci. Phys. 4(1954) 105.
25. Toschev S., Mutaftschiew B.; *On the activity of platinum electrodes during the process of electrolytic nucleation-I*; Electrochimica Acta, 9 (1964): pp. 1203-1210.
26. Scharifker Benjamin and Hills Graham; *Theoretical and experimental studies of multiple nucleation*; Electrochimica. Acta. 28 (1983): pp. 879-889
27. Khelladi M.R, Mentar L, Azizi A, Sahari A, Kahoul A.; *Electrochemical Nucleation and growth of copper deposition onto FTO and n-Si(100) electrodes*; Materials Chemistry and Physics, 115 (2009): pp 385-390.
28. Majidi M.R, Asadpour-Zeynoli K, Hafezi B,; *Reaction and Nucleation mechanisms of copper electrodeposition on disposable pencil graphite electrode*; Electrochimica Acta 54 (2009): pp 1119-1126.
29. Hyde Michael E, Compton Richard G; *A review of the analysis of multiple nucleation with diffusion controlled growth*; Journal of Electroanalytical Chemistry 549 (2003): pp 1-12.
30. Scharifker B.R. and Mostany J.; *Three dimensional Nucleation with diffusion controlled growth*; Journal of Electroanalytical Chemistry, 177 (1984): pp 13-23.
31. Sluyters-Rehbach M, Wijenberg J.H.O.J, Bosco E, and Sluyters J.H.; *The theory of chronoamperometry for the investigation of electrocrystallization*; Journal of Electroanalytical chemistry, 236 (1987): pp 1-20.
32. Heerman Luc., Tarallo Anthony; *Theory of chronoamperometric transient for electrochemical nucleation with diffusion controlled growth*; Journal of Electroanalytical chemistry, 470 (1999): pp 70-76.
33. Gedanken A.; *Using sonochemistry for the fabrication of nanomaterials*; Ultrasonic Sonochemistry, 11 (2004): pp 47-55.
34. Suslick K.; *The chemical effects of ultrasound*; Scientific American, 1989.
35. Sulitanu N, Pirghie C, Brinza F.; *Effect of ultrasound sonication on surface microstructure of the electrodeposited Ni-Zn thin film*; Journal of optoelectronics and advanced materials, 8 (2006): pp. 1889-1891.

36. Walton D. J; *Sonoelectrochemistry-The application of ultrasound to electrochemical systems*; ARKIVOC (2002(iii)) 198-218.
37. Hyde M. E, Compton R. G.; *How ultrasound influence the electrodeposition of metals*; Journal of Electroanalytical Chemistry, 531 (2002): pp 19-24.
38. Rassaei L.; Assembly and Characterization of Nanomaterials into Thin Film Electroanalysis; Doctoral dissertation, University of Kuopio, Kuopio, 2008.
39. Samuel H. G.; Ultrathin Films and Interfacial Phenomena- Comparison of Different Molecular Organization Processes; Doctoral dissertation, University of Saskatchewan Saskatoon, 2003.
40. www.asdlib.org/onlineArticles/elabware/kuwanaEC_lab/PDF-21-Experiment3.pdf
41. Stanjek H., Hausler W.; *Basics of X-Ray Diffraction*; Hyperfine Interactions 154 (2004): pp 107-119
42. *Basics of XRD-Diffraction*; Chapter 7; www.scintag.com,
43. Cullity B. D.; *Elements of X-Ray Diffraction*; Addision-Wesley Publisher, MA, 1978.
44. Voutou B., Stefanaki E.; *Electron Microscopy: The Basics*; Based on Lecture of Dr. Konstantinos Giannakopoulos; Physics of Advanced materials winter School 2008.
45. Goldstein J. I., Newbury D., Joy D., Lyman C., Echlin P., Lifshin E., Sawyer L. and Michael J.; *Scanning electron microscopy and X-Ray microanalysis*; Springer, 2003.
46. Rugar D. and Hansma P.; *Atomic force microscopy*; Physics today, (1990): pp. 23-30.
47. Meyer E.; *Atomic Force Microscopy*; Progress in surface science, 41 (1992): pp. 3-49,
48. Giessib F. J.; *Advanced in atomic force microscopy*; arXiv:cond-mat/0305119v1[cond-mat.mtrl-sci] 6 May 2003
49. Li X., Bhushan B.; *A review of nanoindentation continuous stiffness measurement technique and its applications*; Materials Characterization, 48 (2002): pp 11-36.
50. Chow R., Blindt R., Chivers R., and Povey M.; *A study on the primary and secondary nucleation of ice by power ultrasound*; Ultrasonics, 43, (2005): pp. 227-230
51. Garbellini G. S., Salzar-Banda G. R. and Avaca L. A., Food Chemistry (2009), doi: 10.1016/j. foodchem. 2009-03-069.
52. Gutierrez C. A., Hardcastle J. L., Ball J. C. and Compton R. G., *Anodic stripping voltammetry of copper at insonated glassy carbon- based electrodes: application to the determination of copper in beer*, The Analyst 124,(1999): pp.1053-1057.

53. Floate S., Hyde M. and Compton R. G., *Electrochemical and AFM studies of the electrodeposition of cobalt on glassy carbon: an analysis of the eefct of ultrasound*; Journal of Electroanalytical Chemistry, 523 (2002): pp. 49-63.
54. Gunawardena G, Hills G., Monttenegro I, and Scharifiker B.; *Electrochemivcal nucleation part I general consideration*, Journal of Electroanalytical Chemistry, 138 (1982): pp. 225-239.
55. Godbane O.,Roue L., and Belanger D.; Copper electrodeposition on pyrolytic graphite Electrodes: Effect of the copper salt on the electrodeposition process; Electrochimica Acta, 52 (2007): pp 5843-5855.
56. International Committee for Diffraction Data: Card No. 25-1228.
57. International Committee for Diffraction Data: Card No. 50-1333.
58. Barshilia H. C., and Rajam K. S.; *Characterization of Cu/Ni multilayer coatings by nanoindentation and atomic force microscopy*; Surface and Coatings Technology, 155 (2002): pp 195-202.